have developed a novel method for the immobilization of sulfated oligosaccharide onto a gold-coated SPR chip to prepare a "sugar chip" and devised an analytical system that can be applied to the binding interactions of a variety of structurally defined oligosaccharides in clustered structures that mimic nature.

In this paper, mono-, tri-, and tetravalent types of linker compounds containing one, three, or four aromatic amines and thioctic acid moieties were designed. The ligand moiety, a GlcNS6S-IdoA2S unit, was conjugated with these novel linker compounds to prepare a ligand conjugate using an optimized reductive amination reaction. The ligand conjugates were immobilized on a gold SPR sensor chip through an improved gold−sulfur (Au−S) permanent bond. By this approach, we were able to accurately measure the specific interactions of the GlcNS6S-IdoA2S structure in heparin with native human vWf protein and with the recombinant fragment of its A1 domain. To compare our method with conventional immobilization techniques, the GlcNS6S-IdoA2S unit was conjugated with a hydrophobic aromatic amine by a similar reductive amination reaction and immobilized through hydrophobic interactions with a hydrophobic 1-octanethiol-coated chip surface.

The goal of this current work was to refine the methods for immobilizing clustered oligosaccharides using these new techniques, to measure their uniformity and distribution on the SPR chip, and to measure the relative impact of ligand clustering on the binding of well-known heparin-binding proteins. Our long-term goal is to provide a simple, versatile, and reproducible method for studying glycosaminoglycan−protein interactions, which can be implemented by a wide range of investigators beyond the specialized laboratories that pioneered these approaches.

EXPERIMENTAL PROCEDURES

General Procedure. All reactions in organic media were carried out with freshly distilled solvents or with commercially available extra grade solvents purchased from Kanto Chem. Co. (Tokyo, Japan), Nacalai Tesque (Kyoto, Japan), or Wako Chem. Co. (Osaka, Japan). Silica gel column chromatography was performed using silica gel 60 (no. 9386, Merck & Co. Inc., Whitehouse Station, NJ). Spectral data were obtained as follows. Electrospray ionization time-of-flight mass (ESI-TOF/MS) spectra were obtained by Mariner (Applied Biosystems, Framingham, MA). ^{1}H NMR measurements were performed with JEOL (Tokyo, Japan) Lambda-500, GSX-400, and ECA-600. The chemical shifts are expressed in δ-values using tetramethylsilane (δ 0) or HDO (δ 4.65) as an internal standard.

SPR Experiments. SPR experiments were perfomed with SPR-670 (Nippon Laser and Electric Lab., Nagoya, Japan) under the recommended manufacture's guideline with a slight modification. Sensor chips used for SPR experiments were prepared as follows. The gold-coated chip was purchased from Nippon Laser and Electronics Lab. For ligand conjugates containing the thioctic acid moiety, the gold-coated chip was soaked in a 100 μM solution (methanol/water = 1/1, v/v) of the appropriate ligand conjugate at room temperature for 2 h or overnight, followed by subsequent washing with methanol/water containing 0.05% Tween-20, phosphate-buffered saline (PBS) at pH 7.4 containing 0.05% Tween-20, and PBS (pH 7.4). All washings were done with microwave irradiation for 5−30 min. The solvent for the binding experiment was PBS at pH 7.4 and run at a flow rate of 15 μL/min at 25 °C.

For ligand conjugates containing an octyl group, the gold chip was first soaked in 1 mM methanol solution of octanethiol at room temperature overnight, followed by washing with methanol, methanol/water (1/1, v/v), and PBS (pH 7.4) containing 10% 2-propanol. The octanethiol immobilized chip (self-assembled monolayer (SAM) chip) was set in the SPR-670; then the solution of ligand conjugate containing the octyl group in PBS (pH 7.4) containing 10% 2-propanol was loaded and run at a flow rate of 15 μL/min at 25 °C. The ligand conjugate became immobilized through a hydrophobic interaction between the SAM on the chip and the octyl group of the conjugate. This was monitored by SPR-670. The subsequent saccharide−protein binding experiments were done using PBS (pH 7.4) containing 10% 2-propanol. Bovine serum albumin (BSA) was employed as the control, nonspecific protein of study. It is ubiquitous in biological systems and is known to have low nonspecific interactions with sulfated polysaccharides.

Synthesis of Compounds. Details of compound syntheses can be found in Supporting Information.

RESULTS

Preparation of Oligosaccharide-Linker Conjugates (Abbreviated as "Ligand Conjugates"). Mono-, tri-, and tetravalent linker molecules and ligand conjugates were prepared as illustrated in Schemes 1−5. The linker compounds possessed one, three, or four incorporating points, and the ligand conjugates were composed of the linker attached to a structurally defined, biologically active sulfated disaccharide unit (GlcNS6S-IdoA2S) or D-glucose as a control. All the structures of the compounds were confirmed by ESI-TOF/MS and NMR.

Monovalent Linkers and Ligand Conjugates (Schemes 1 and 2). The reaction of *m*-phenylenediamine **1** with di-*t*-butyl dicarbonate in methanol solution yielded 3-(*t*-butoxycarbonylamino)phenylamine **2**. The compound **2** was then reacted with thioctic acid **3** in dichloromethane to give the thioctamide derivative **4**, followed by treatment with trifluoroacetic acid to yield the linker compound **5**. A reductive amination reaction with a sulfated trisaccharide **6** (synthesized as previously reported (*18*)) was employed to incorporate the disaccharide unit into a novel ligand conjugate **7** (Mono-GlcNS6S-IdoA2S-Glc). By a similar reductive amination reaction using D-glucose, a control ligand conjugate **8** (Mono-Glc) was also prepared.

For the hydrophobic immobilization strategy (Scheme 2), a hydrophobized ligand conjugate **13** containing the GlcNS6S-IdoA2S unit was prepared. The reaction of 4-aminobenzoic acid **9** with di-*t*-butyl dicarbonate in methanol solution yielded 4-(*t*-butoxycarbonylamino)benzoic acid **10**. Further reaction with *n*-octylamine in dichloromethane gave benzamide **11**, which was then treated with trifluoroacetic acid to yield the hydrophobic linker *N*-octyl-4-aminobenzamide **12**. The linker **12** was coupled with the trisaccharide **6** using a reductive amination reaction to give the hydrophobized compound **13** (Hydro-mono-GlcNS6S-IdoA2S-Glc). A similar reductive amination was performed with D-maltose to give D-glucopyranoside-containing ligand conjugate **14** (Hydro-mono-Glc-Glc), which was used for the control experiments.

Trivalent Linker and Ligand Conjugate (Scheme 3). For the trivalent type linker compound **24**, the Michael addition reaction followed by reduction with Raney nickel was applied to nitromethane **15** to give tribranching amine **18** according to Weis and Newkome (*19*) with a slight modification. The production of a side product, di-*t*-butyl 4-[(2-*t*-butoxycarbonyl)ethyl]-4-aminoheptanedicarboxylate, was less than 5% in this case. To the amine moiety **18**, a *Z*-glycine unit was incorporated, which served as a spacer between the branching part and the further incorporating thioctic acid moiety. The coupling reductive amination reaction was performed as above with a slight modification, in which dimethylacetoamide was used to dissolve the tribranched linker compound **24** instead of methanol. The reaction was monitored with thin-layer chromatography (TLC) and ESI-TOF/MS. After confirmation of the formation of the Shiff base, the ratio of the mixed solvent was changed to promote a more efficient reduction reaction. We found that it

Scheme 1. Synthesis of Monovalent Linker and Ligand Conjugates

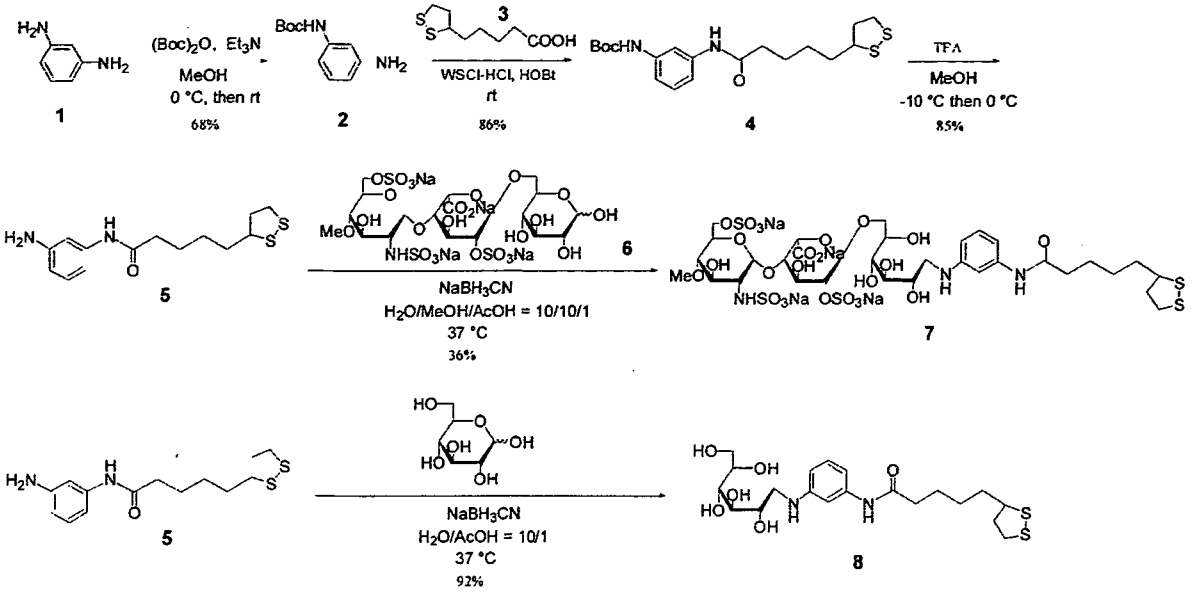

Scheme 2. Synthesis of Hydrophobized Monovalent Linker and Ligand

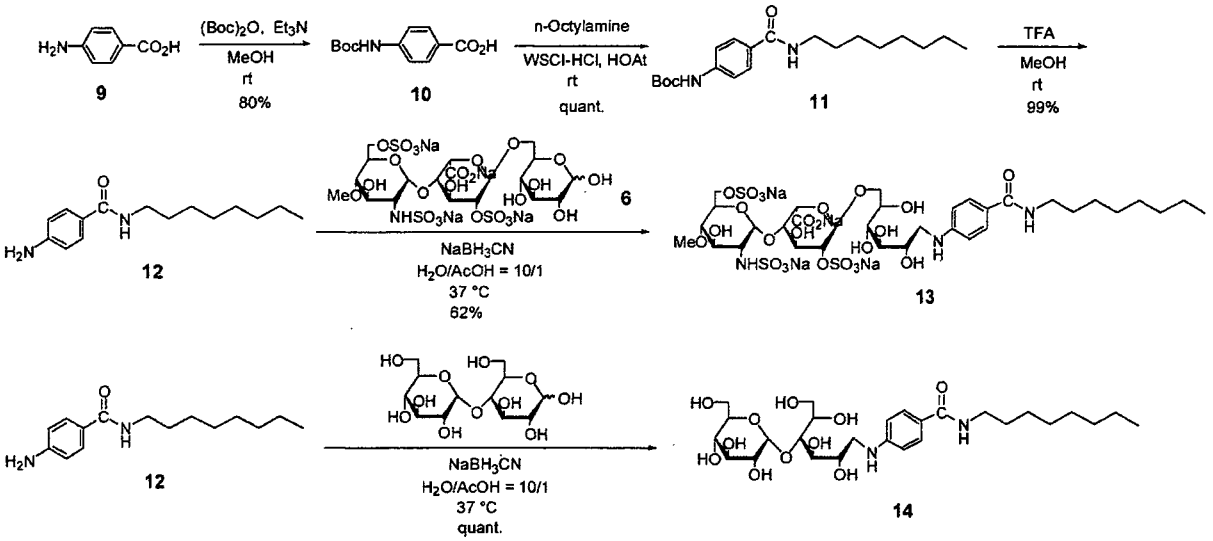

was important to maintain the pH of the solvent between 3 and 4 to increase the conversion of the reaction. A 5-fold ratio of sulfated trisaccharide **6** to the linker **24** was necessary to incorporate all three of the aromatic amine moieties in **24** to produce **25** (Tri-GlcNS6S-IdoA2S-Glc). The lower than expected yield (66%) was due to losses during purification.

Tetravalent Linker and Ligand Conjugate (Scheme 4). The tetravalent linker compound **34** was prepared according to Ashton et al. (*20*) with modifications. In brief, two units of aminobenzoic acid moieties were incorporated into the two primary amines in diethylenetriamine with a relatively good yield by precisely controlling their molar ratio. For the spacer between the thioctic acid moiety and the branching part, *Z*-glycine was incorporated to give compound **30**. The condensation of **27** and **31** needed a stronger condensation reagent, pentafluorophenyl diphenylphosphinate (FDDP), to give the tetravalent linker unit containing four units of aromatic amine derivative **35**. The incorporation of sulfated disaccharide units to yield **35** was performed by similar reaction conditions as applied to **24**. A 5-fold ratio of sulfated trisaccharide **6** to the linker **35** was also necessary to incorporate all four of the aromatic amine moieties in **35** to produce **36** (Tetra-GlcNS6S-IdoA2S-Glc-short). Diminished yield (40%) was again due to losses during purification.

Tetravalent Linker and Ligand Conjugate with Longer Spacer Arm (Scheme 5). In order to create an immobilized oligosaccharide cluster with a longer leash, or spacer arm, we created tetravalent linker **48** and ligand conjugate **49** by modifying **35** and **36**, respectively (Scheme 5). An oligo(ethylene glycol) unit was incorporated between the branched part and the thioctic acid moiety. The oligo(ethylene glycol) unit was derivatized according to Houseman and Mrksich (*6*) to afford the *O*-toluenesulfonyl compound **40**. By the S_N2 reaction with sodium azide, an azide unit was incorporated. After hydrolysis, we obtained **42**, which was then used for the spacer unit instead of *Z*-glycine in the preparation of **30**. The azide moiety was converted to amine by mild reduction, and the thioctic acid moiety was condensed to the amino group, followed by deblocking of the aromatic amine by trifluroacetic acid to yield the tetravalent linker **48** containing an oligo(ethylene glycol)

Scheme 3. Synthesis of Trivalent Linker and Ligand Conjugate

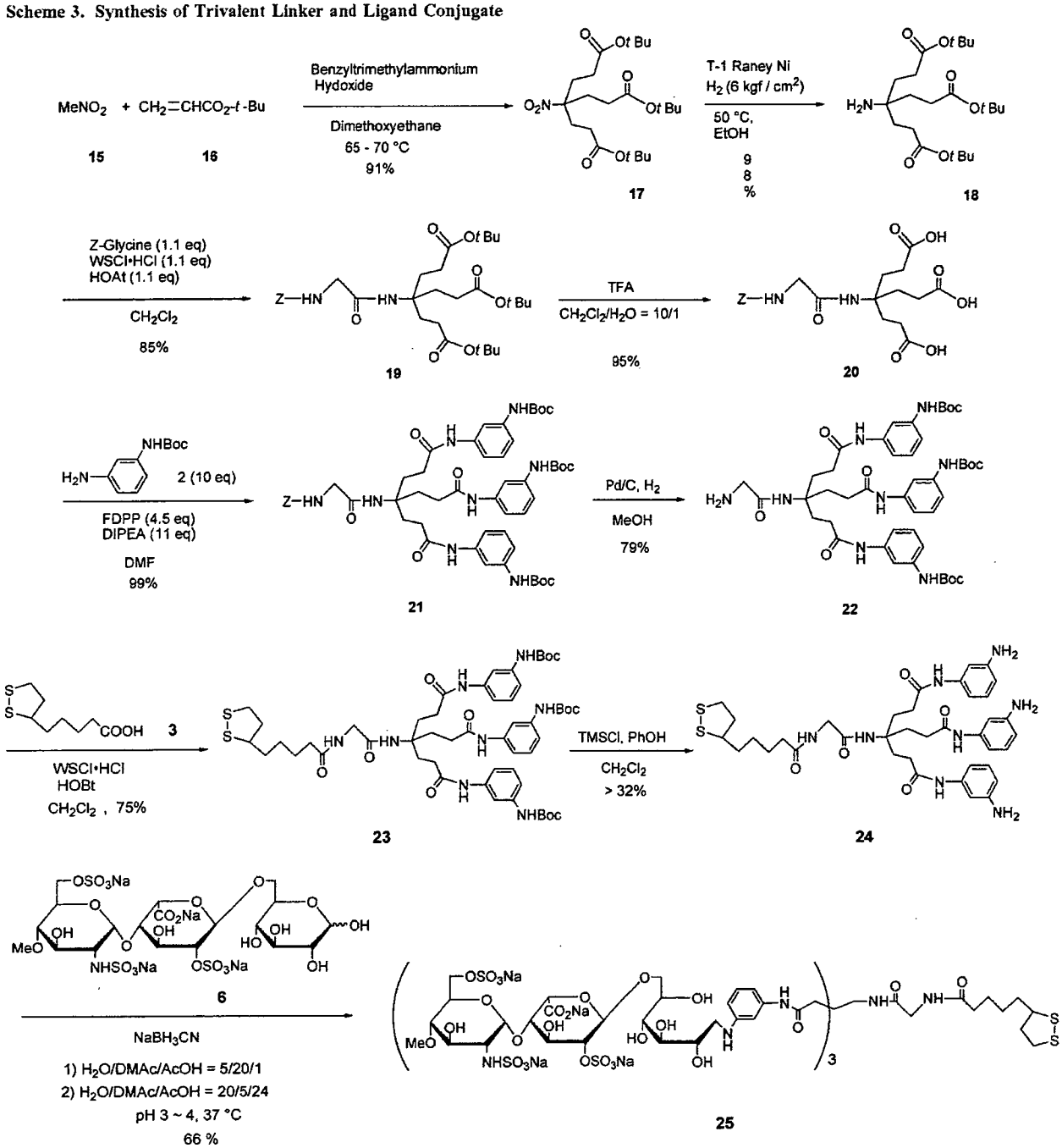

unit. The incorporation of sulfated disaccharide units into **48** was performed by the same reaction as applied to **25**. A 7-fold ratio of sulfated trisaccharide **6** to the linker **48** was necessary to incorporate the four aromatic amine moieties in **48** to prepare **49** (Tetra-GlcNS6S-IdoA2S-Glc-long). Yield (22%) was again diminished primarily due to purification. All the structures of the compounds were confirmed by ESI-TOF/MS and ^{1}H NMR.

Comparison of Immobilization Methods. The monovalent ligand conjugates **7** (Mono-GlcNS6S-IdoA2S-Glc) and **8** (Mono-Glc) were first immobilized on the gold chip by soaking the chip in the 100 μM 50% aqueous methanol solution of the ligand conjugate for 2 h or overnight at room temperature with gentle agitation. It was predicted that the ligand conjugates would be immobilized on the gold-coated chip through direct Au−S bonding. With use of an SPR670 apparatus (Nippon Laser and Electronics Lab, Nagoya, Japan), a binding interaction to the ligand moiety on the chip was confirmed when 2 μM of the synthetic peptide KDRKRSELRRIASQVK (a discrete heparin-binding domain of human vWf (*21*), abbreviated as vWf-peptide) was injected over the surface of the chip in the apparatus (Figure 1a). Because minimal binding was observed with 1.5 μM of BSA, it was not even necessary to subtract a nonspecific binding value.

When the control Mono-Glc was immobilized using the same method, no significant increase in resonance units was observed even though a high concentration of synthetic vWf-peptide was used (Figure 1b). In contrast, a typically positive binding saturation curve was seen with the Mono-GlcNS6S-IdoA2S-

Scheme 4. Synthesis of Tetravalent Linker Containing Short Spacer Arm and Ligand Conjugate

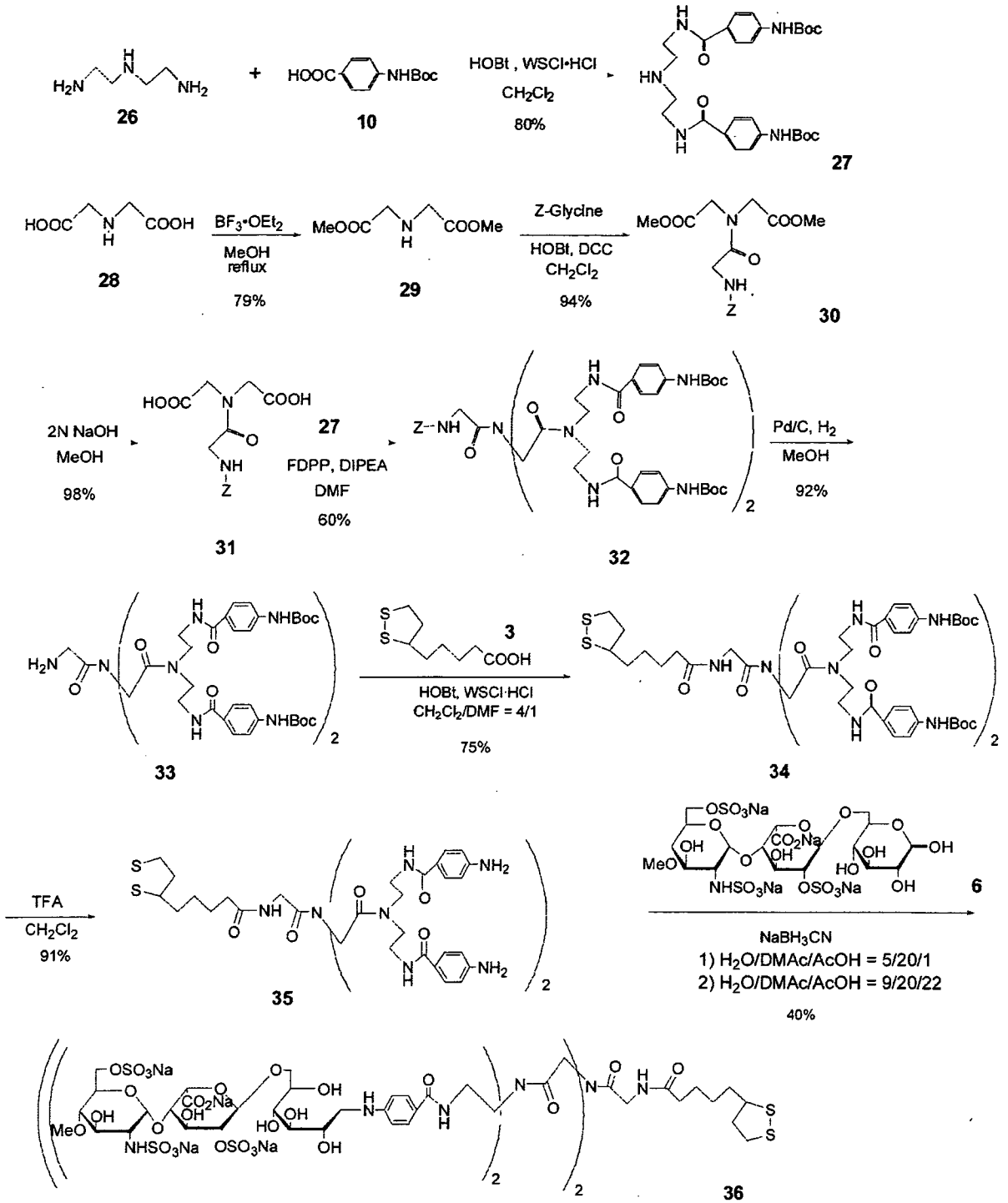

Glc immobilized chip. The K_D, dissociation constant, was estimated to be 220 nM, very close to that reported previously (370 ± 100 nM) for unfractionated heparin and vWf using a conventional radioligand binding assay (*21*).

This direct, covalent immobilization method was then compared to a conventional hydrophobic method of immobilization. A self-assembled monolayer (SAM) of octanethiol was first prepared on the chip as previously reported (*10*, *11*). The SAM chip was set in the SPR670 apparatus and a solution of **13** or **14** was loaded on the chip in phosphate-buffered saline. The total amount of **13** or **14** that was immobilized on the sensor chip is indicated by the differences in resonance units (ΔRU^1) at equilibrium shown in Figure 2a. Then, the binding of synthetic vWf-peptide was evaluated. Figure 2b shows that the vWf-peptide bound to both the sulfated oligosaccharide SAM chip (using **13**, Hydro-mono-GlcNS6S-IdoA2S-Glc) and the control SAM chip (using **14**, Hydro-mono-Glc-Glc). These nonspecific interactions were confirmed when BSA was tested on the same SAM sensor chip; strong binding of BSA to both chips was observed (data not shown).

Scheme 5. Synthesis of Tetravalent Linker Containing Long Spacer Arm and Ligand Conjugate

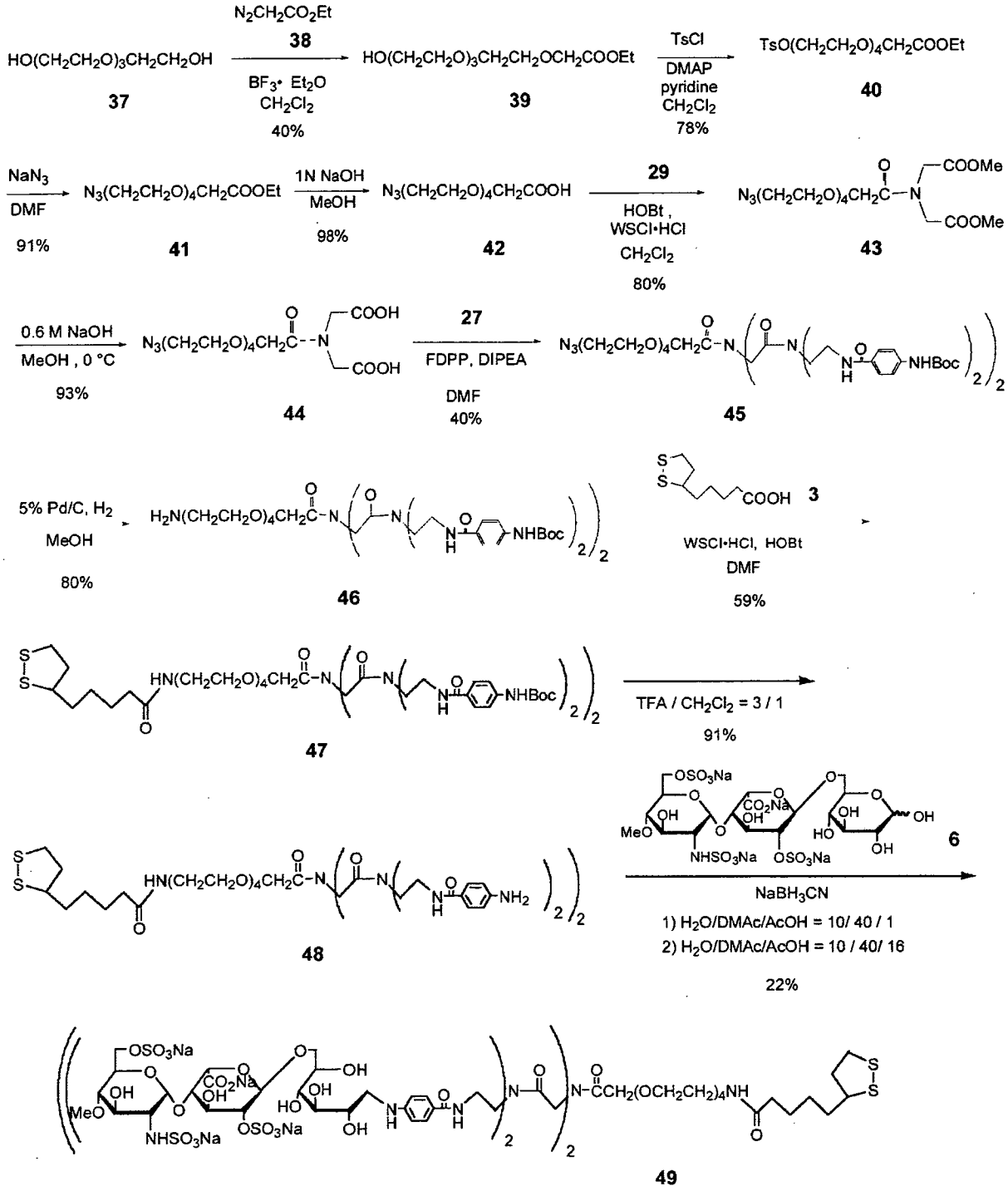

Evaluation of Immobilization of the Ligand Conjugates via the Covalent Attachment Method. The tri- and tetravalent ligand conjugates containing the sulfated disaccharide units were immobilized on gold chips as described above, and nonspecific binding to 1.5 μM BSA was measured. Experience showed that the chips prepared in this manner were quite stable, retaining full binding potency when stored dry at room temperature for 6 months (data not shown). Figure 3 shows that chips immobilized with conjugates **25** (Tri-GlcNS6S-IdoA2S-Glc) and **49** (Tetra-GlcNS6S-IdoA2S-Glc-long) showed very little nonspecific binding, just as was observed in Figure 1a with the Mono-GlcNS6S-IdoA2S-Glc (conjugate **7**). The tetravalent conjugate with the short linker arm (conjugate **36**) exhibited high nonspecific binding (Figure 3) that is typical of a BSA interaction with a bare, unmodified gold chip. Hence, we concluded that conjugate **36** did not achieve optimal immobilization to the gold chip. Its more flexible linkage chemistry, combined with a short spacer arm, may have obscured the accessibility of the S−S portion of the linker for effective immobilization. In subsequent experiments, trivalent

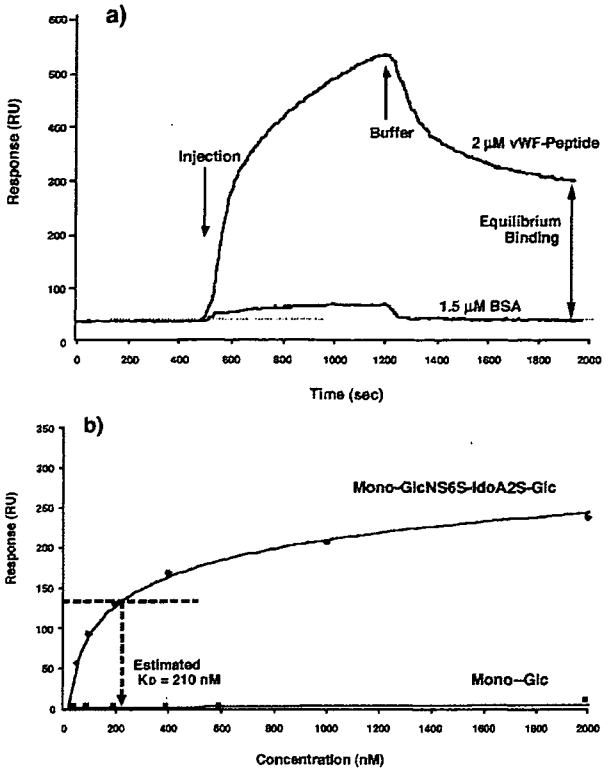

Figure 1. (a) Binding of vWf-peptide and BSA to Mono-GlcNS6S-IdoA2S-Glc (ligand conjugate 7) on the chip was observed (flow rate = 5 μL/min, temp = 25 °C, pH 7.4, PBS); (b) the equilibrium binding data were used to generate a saturation curve for vWf-peptide binding to Mono-GlcNS6S-IdoA2S-Glc and to the control ligand conjugate 8 (Mono-Glc).

ligand conjugate **25** (Tri-GlcNS6S-IdoA2S-Glc) and ligand conjugate **49** (Tetra-GlcNS6S-IdoA2S-Glc-long) were used in addition to Mono-GlcNS6S-IdoA2S-Glc (compound **7**).

Density and Homogeneity of Immobilization. We wished to determine how the density of immobilization of different conjugates on the chip would influence binding activity. Accordingly, different percentages of biologically active ligand conjugates were individually diluted with the control glucose monovalent conjugate **8** (Mono-Glc) and immobilized as above. The relative concentration of the immobilized sulfated disaccharide was determined by attenuated total reflection (ATR) FT-IR spectra with IRPrestige-21 equipped with MIRacle (Shimdzu Co., Kyoto, Japan). Figure 4a shows parts of the ATR-FT-IR spectra for the region of sulfate groups (1200 and 1303 cm^{-1}) on the gold surface, where Mono-GlcNS6S-IdoA2S-Glc was immobilized over a range of relative densities. The intensity of absorbance increased as the chip was coated with an increasing percentage of Mono-GlcNS6S-IdoA2S-Glc in the ligand conjugate mixture. The absorbance between 1200 and 1303 cm^{-1} was integrated and plotted against the relative concentration of ligand conjugate including the sulfated disaccharide units. As shown in Figure 4b–d, there were linear relationships between the integral of absorbance for sulfate groups on the chip and the relative concentration of the active ligand conjugate in the mixture, suggesting that the sulfated disaccharide units were homogeneously immobilized on the gold surface. In other words, the relative density of ligand oligosaccharides on the chip surface can be controlled by admixing the Mono-Glc ligand conjugate, since the efficiency of S–Au bonding does not appear to be altered between Mono-GlcNS6S-IdoA2S-Glc and Mono-Glc.

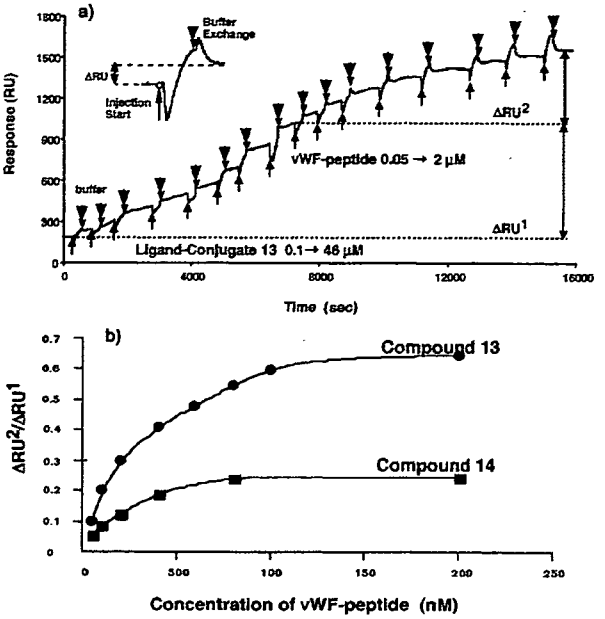

Figure 2. (a) Immobilization of ligand conjugate **13** (Hydro-mono-GlcNS6S-IdoA2S-Glc) containing GlcNS6S-IdoA2S on the SAM chip and the binding of vWf-peptide were observed (flow rate = 15 μL/min, temp = 25 °C, pH 7.4, PBS containing 10% 2-propanol); (b) the equilibrium binding data were used to generate saturation curves for the binding of vWf-peptide to the ligand conjugate **13** and to the control **14** (Hydro-mono-Glc-Glc).

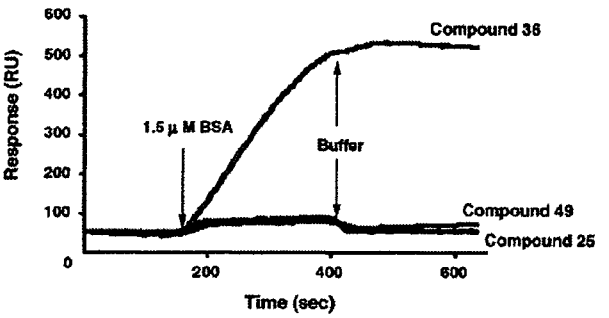

Figure 3. Binding of BSA to the sulfated disaccharide, GlcNS6S-IdoA2S, immobilized chips by ligand conjugates **25** (Tri-GlcNS6S-IdoA2S-Glc), **36** (Tetra-GlcNS6S-IdoA2S-Glc-short), and **49** (Tetra-GlcNS6S-IdoA2S-Glc-long). The immobilization and SPR experiment were done as described in the Experimental Procedures.

Measurement of Binding Affinities for Model Heparin-Binding Proteins. To evaluate the influence of oligosaccharide immobilization density on protein binding, 2 μM vWf-peptide was injected over chips immobilized with different percentages of Mono-GlcNS6S-IdoA2S-Glc to Mono-Glc immobilized chip (Figure 5). The binding affinity decreased as the relative density of the surface-immobilized sulfated disaccharide units diminished. When the biologically active disaccharide comprised less than 40% of the immobilized ligand, binding was minimal.

We also studied the binding of the recombinant human vWf-A1 domain (rhvWf-A1) (*22*). This protein contains the same heparin-binding domain studied in Figure 5 (vWf-peptide) but also includes a secondary or cooperative heparin binding site (*23*). The three ligand conjugates, Mono-GlcNS6S-IdoA2S-Glc, Tri-GlcNS6S-IdoA2S-Glc, and Tetra-GlcNS6S-IdoA2S-Glc-long, were immobilized at 100% and 50% density (mixed 1:1 with Mono-Glc). Table 1 compares the effects of clustering (valency) and immobilization density on the binding parameters

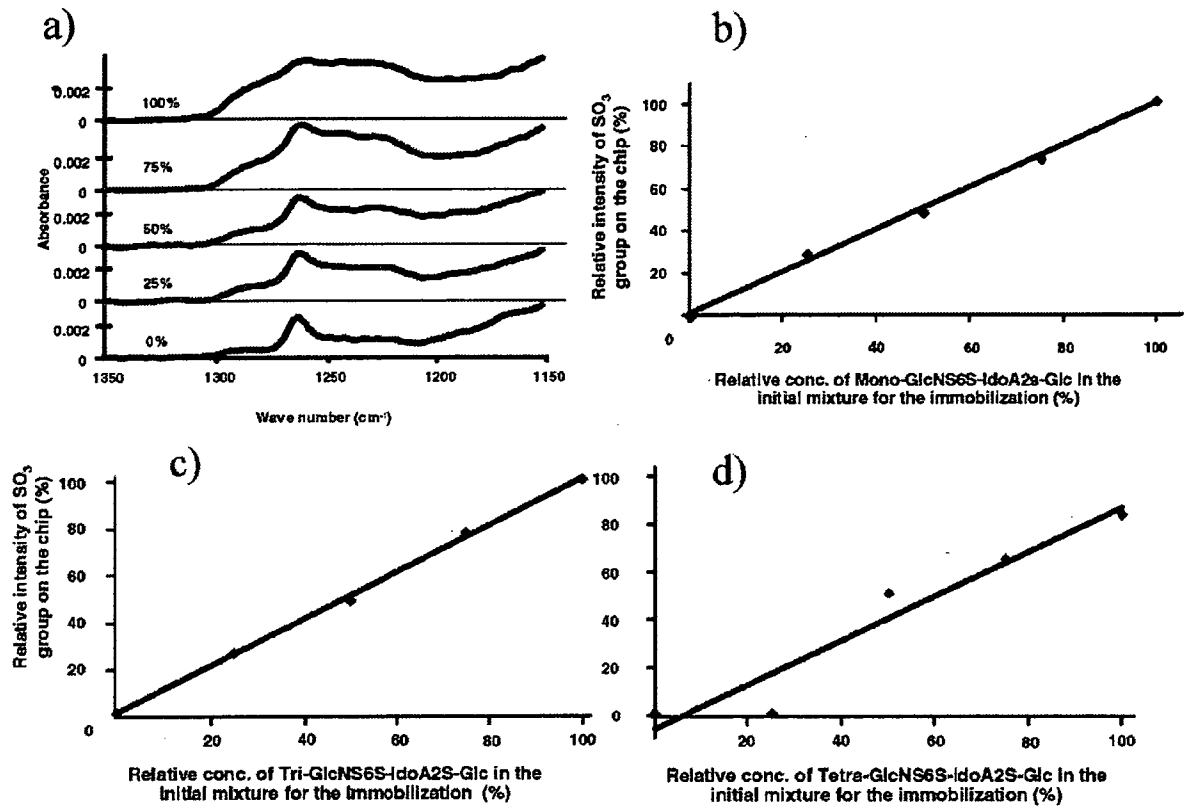

Figure 4. (a) ATR-FT-IR spectra of Mono-GlcNS6S-IdoA2S-Glc immobilized chip. The immobilization was done by adding Mono-GlcNS6S-IdoA2S-Glc to the control ligand conjugate (Mono-Glc) with changing concentration (0 to 100%). Intensity of ATR-FT-IR was plotted against the initial concentration of (b) Mono-GlcNS6S-IdoA2S-Glc (R^2 = 0.9984), (c) Tri-GlcNS6S-IdoA2S-Glc (compound **25**; R^2 = 0.9993), and (d) Tetra-GlcNS6S-IdoA2S-Glc-long (compound 49; R^2 = 0.9610) in the ligand conjugate mixture.

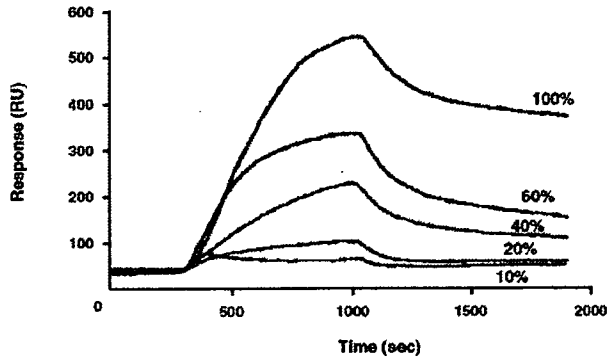

Figure 5. SPR sensorgram of vWf-peptide binding. Chips were immobilized with increasing proportions of Mono-GlcNS6S-IdoA2S-Glc, with the total concentration ([Mono-GlcNS6S-IdoA2S-Glc] + [Mono-Glc]) fixed at 100 μM. vWf-peptide was 2 μM.

(calculated from kinetic data using the analytical software of the SPR670).

The increased clustering of oligosaccharides provided by the tri- and tetravalent conjugates uniformly yielded lower dissociation constants K_D and lower dissociation rates k_d. The monovalent conjugate had an ~2.5−3-fold higher K_D and k_d. A 50% decrease in the density of immobilization hardly changed the binding parameters of the tri- and tetravalent ligand conjugates, while the same decrease in density of the monovalent ligand raised the K_D by 1.5-fold and doubled the k_d.

We then measured oligosaccharide binding of an even more complex version of this heparin-binding protein, the whole human vWf protein. A single vWf monomer protein is 270 kDa

Table 1. Binding of rhvWf-A1: Clustering Effect of Sulfated Oligosaccharide on the Chip

ligand conjugates	ratio	K_D [a] (μM)	k_a [b] ($M^{-1}\,s^{-1} \times 10^3$)	k_d [c] ($s^{-1} \times 10^{-3}$)
Mono-GlcNS6S-IdoA2S-Glc	100/0	2.60	8.38	21.9
Mono-GlcNS6S-IdoA2S-Glc/ Mono-Glc	50/50	3.79	14.6	55.2
Tri-GlcNS6S-IdoA2S-Glc	100/0	1.20	6.60	8.05
Tri-GlcNS6S-IdoA2S-Glc/ Mono-Glc	50/50	1.50	4.52	6.83
Tetra-GlcNS6S-IdoA2S-Glc	100/0	0.99	6.50	6.44
Tetra-GlcNS6S-IdoA2S-Glc/ Mono-Glc	50/50	1.00	5.24	5.26

[a] k_d/k_a (dissociation constant). [b] Association rate. [c] Dissociation rate.

Table 2. Binding of Whole rhvWf: Lack of Clustering Effect of Sulfated Oligosaccharide on the Chip

ligand conjugates	ratio	estimated K_D (nM)
Mono-GlcNS6S-IdoA2A-Glc	100/0	35
Mono-GlcNS6S-IdoA2A-Glc/Mono-Glc	20/80	41
Tri-GlcNS6S-IdoA2A-Glc	100/0	24
Tri-GlcNS6S-IdoA2A-Glc/Mono-Glc	20/80	27
Tetra-GlcNS6S-IdoA2A-Glc	100/0	35
Tetra-GlcNS6S-IdoA2A-Glc/Mono-Glc	20/80	32

molecular mass, but it forms large multimers reaching several million daltons, displaying multiple heparin-binding sites. Experiments were performed using mono-, tri-, and tetravalent (long) ligand conjugates immobilized at 100% and 20% relative concentrations. Table 2 summarizes the estimated binding constants derived from the data illustrated in Figure 6a−c. The estimated K_D values were all very similar and did not depend

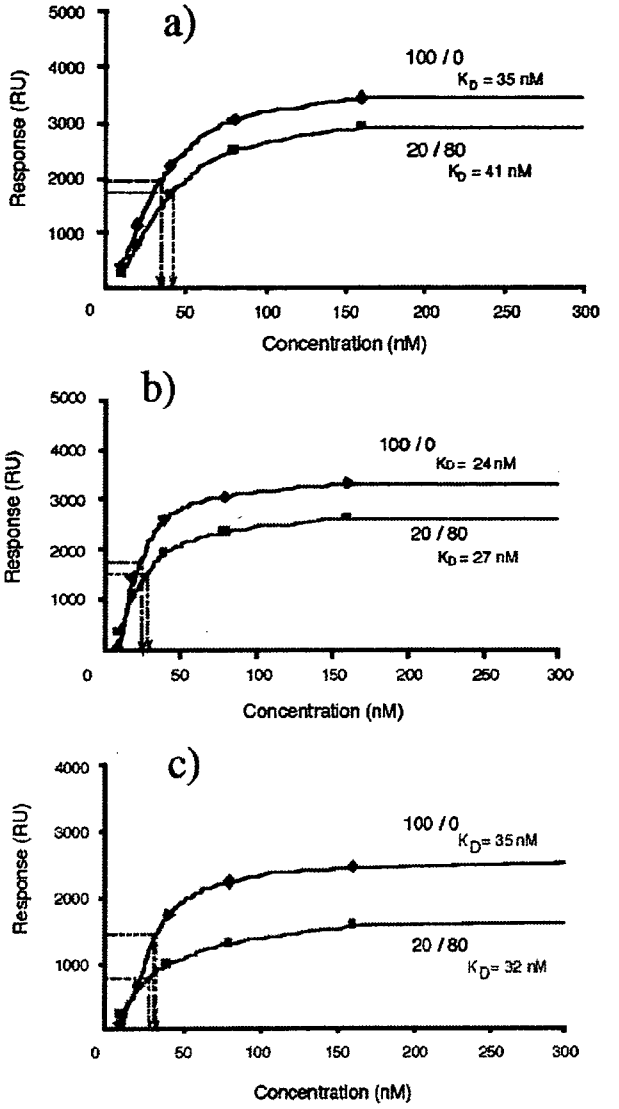

Figure 6. Equilibrium binding of whole hvWf protein to chips immobilized with Mono-GlcNS6S-IdoA2S-Glc/Mono-Glc (a), Tri-GlcNS6S-IdoA2S-Glc/Mono-Glc (b), and Tetra-GlcNS6S-IdoA2S-Glc-long/Mono-Glc (c). The ratios of Mono-GlcNS6S-IdoA2S-Glc, Tri-GlcNS6S-IdoA2S-Glc, or Tetra-GlcNS6S-IdoA2S-Glc-long/Mono-Glc were 100/0 and 20/80.

on the relative density of the immobilization of the ligand conjugates nor the multivalency of the ligand conjugate.

Finally, we studied the binding affinity for a completely different heparin-binding protein, human basic fibroblast growth factor (bFGF). Here we performed competitive binding studies with immobilized Tri-GlcNS6S-IdoA2S-Glc (compound **25**) and bFGF (200 nM) in solution phase admixed with increasing concentrations of unfractionated pharmaceutical grade heparin (Nacalai Tesque, from porcine intestine, average MW = 15000). Figure 7a shows that with increasing concentrations of soluble heparin, the binding of 200 nM of bFGF decreased. Figure 7b shows the estimated IC_{50} of heparin to be 50−100 nM, which is close to the reported K_D of bFGF for heparan sulfate proteoglycan (*24*).

DISCUSSION

The first goal of this work was to devise and refine a simpler and nondestructive strategy for immobilizing structurally defined

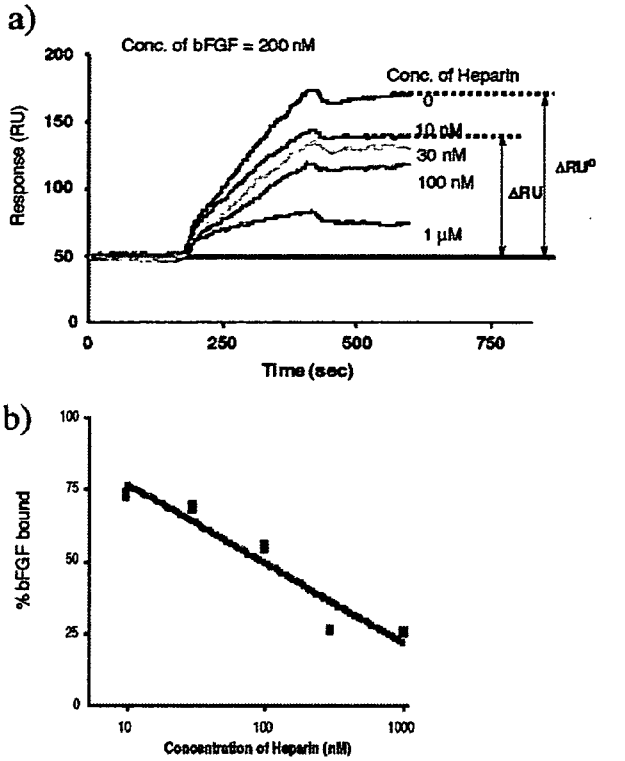

Figure 7. (a) SPR sensorgram of competitive heparin binding to bFGF. Mixtures of bFGF (200 nM) with or without soluble commercial heparin (Nacalai Tesque, from porcine intestine, average MW = 15000) were run on the chip of Tri-GlcNS6S-IdoA2S-Glc. (b) Relationship between the concentration of heparin and ΔRU at equilibrium.

oligosaccharides on a chip for SPR. When ligand immobilization methods were compared, the direct, covalent immobilization to the gold surface via Au−S bonds yielded minimal nonspecific binding interactions, as examplified by the negligible binding of BSA, and minimal protein binding to the control glucose ligand. In contrast, BSA bound to the self-assembled monolayer of octanethiol through nonspecific hydrophobic interactions, and the vWf-peptide bound with some measurable affinity even to the negative control glucose ligand.

We also sought to develop a linkage method that was simple, nondestructive, and applicable to a wider range of naturally occurring oligosaccharides. The reductive amination coupling to linker compounds containing aromatic amines offered more precise, quantitative control over the linkage process, especially when compared with techniques of mass immobilization using the lysine groups of albumin or other proteins. The reductive amination reaction is certainly a well-established method. It is typically used for the labeling of oligosaccharides, such as in the pyridyl amination reaction. In that case, excess amounts of pyridylamine are used, and the labeled compounds have been used primarily for the analysis of the structure of oligosaccharides. With use of this known pyridyl amination reaction, ligand conjugates for the immobilization of oligosaccharides onto the gold surface cannot be obtained.

Other methods have used the amino groups in a carrier protein, like bovine serum albumin, to form multivalent ligand oligosaccharides with dramatic increases in binding affinity. We previously examined the reductive amination strategy in detail and found the optimized conditions (*25*). In brief, the reaction should be done at around pH 4 to get a high yield. Therefore, regular alkyl amines gave lower yields because of the protonation of the amino group. If the pH is increased to over seven to have more free amino groups, the simple reduction at the

reducing end of oligosaccharide predominated. Thus, we found that aromatic amines had the optimal properties. Using those linker compounds described here, many other oligo- and polysaccharides including sialic containing ones, unfractionated high molecular weight heparin, low molecular weight heparins (LMWHs) prepared by several different methods, or amyloses, were also successfully conjugated. Those results will be reported soon.

Gold−sulfur immobilization schemes have also been used by Ratner et al. (*26*) and Horan et al. (*5*), but the regular thiol-containing compounds they used for self-assembling monolayers can form both S−S and S−H bonds, depending on the concentration. Therefore, purification of these oligosaccharide−thiol conjugates may be challenging, with low yields. Our current approach using a linker compound containing a thioctic acid with intramolecular S−S bonds avoids these significant challenges in purification during the synthesis. The advantages of using thioctic acid have been recognized in our patent (*27*) and in a recent publication (*28*).

The second purpose was to precisely quantify the nanostructural contributions of clustering, or valency, on the affinity of oligosaccharide ligands for increasingly complex heparin-binding proteins by varying spacer-arm length, immobilization density, and valency. Here, the distinction should be made between the minimal oligosaccharide binding unit and the minimal functional oligosaccharide necessary for biological activity. Often, a di- or trisaccharide of specific structure can be identified as the key binding unit (as we have done previously (*17*)). However, an isolated disaccharide often has low affinity and biological activity for the target protein. When multiple copies of this minimal binding unit are spaced appropriately (either within a single heparin chain or by adjacent chains), then the ligand protein may engage in higher affinity equilibrium binding that results in biological effects. Thus, overall the tri- or tetravalent compounds had higher affinities than the monovalent type, and the affinity was less dependent on their relative density on the surface of the SPR gold chip (Table 1). That is, when multivalency was incorporated as an intrinsic property of the ligand, variations in the density of immobilization had significantly less effect on the observed affinities. In contrast, the affinities of the monovalent ligand conjugates dropped dramatically when their relative density fell to 50%. Even though the changes shown in Table 1 were small, we observed a larger increase of K_D (lower affinity) of rhvWf-A1 when the relative density was decreased to 20% (data not shown). A larger k_d rate constant (Table 1) was observed compared to 100% density, suggesting that the observed binding of rhvWf-A1 occurred via equilibrium binding. These results support the concept that oligosaccharide ligand valency and density are important determinants for protein affinity. In biological systems, the key minimal oligosaccharide structure may either be spaced appropriately as a repeating unit within the same polymer chain or be displayed by clusters of neighboring polymers.

In addition to intrinsic ligand valency and density, it was interesting to find that a third factor also influenced equilibrium binding, the complexity of the heparin-binding protein. In the case of the simplest monovalent disaccharide ligand conjugate, its binding to a single, linear heparin-binding domain peptide (vWf-peptide) was highly dependent on the density of immobilized ligand (Figure 5). The monovalent ligand's interaction with a more complex heparin-binding protein (rhvWf-A1 containing major and minor heparin-binding domains) was still dependent on immobilization density, but slightly less so (Table 1). Finally, the monovalent ligand's interaction with the native multimeric vWf protein (containing multiple heparin-binding sites) showed the least dependency on immobilization density (Table 2). The binding of multivalent oligosaccharide ligands to increasingly complex heparin-binding proteins was much less sensitive to immobilization density. The trivalent and tetravalent constructs with the long spacer arm exhibited no significant change in K_D with reduced density.

Microarrays of synthetic heparin oligosaccharides have been reported very recently (*29*). But from these "sugar chips", the influence of the heparin-binding protein lends insights into the nature of protein−glycosaminoglycan binding mechanisms. It suggests that as the protein presents a multiplicity of heparin-binding sites, the interactions with the sulfated disaccharide units change from static multipoint binding to kinetic equilibrium binding. Neither ligand clustering nor density seemed to play as important a role in binding native multimeric hvWf, most likely because of the many widely spaced ligand binding sites presented by the protein itself. These results point to one unexpected advantage of this current technology: by altering the relative density and valency of the ligand on the surface, one can easily distinguish between single-site and multisite binding interactions between proteins and oligosaccharides. Thus, the heparin-binding properties of an unknown protein can be deduced.

Another utility of this approach is illustrated by the competitive binding assay using the trivalent ligand conjugate and human bFGF. We measured similar competition curves by soluble heparin against the monovalent or tetravalent ligand conjugates (data not shown). This technique can be easily applied, for example, to the screening of inhibitors or competitors of growth factors.

In previous work, we have found that the surface of the commercial gold-coated chip, at nanometer scale, is not perfectly flat. It varies in vertical elevation by as much as 10 nm up and down (detected by atomic force microscopy (AFM), data not shown). Thus, it was not surprising that the immobilization of ligands less than 2 nm in size might be affected by surface conditions, producing less consistent two-dimensional clustering of ligand on the surface. However, in the tri- or tetravalent type ligand conjugates, the biologically active oligosaccharides were dispersed within 2−3 nm, making a nanometer-sized cluster, which is independent of the surface irregularities of the gold-coated chip. Up to a point, a clustering-type effect can be achieved by immobilizing monovalent ligands at a higher density, but the nanostructural properties of the surface may interfere with the consistency and reproducibility of this effect. One explanation may be that the multivalent linkers are less affected by these surface conditions and thus show comparable affinities at lower density. Among them, the trivalent type may have some advantages. The trivalent linker contains an sp^3 carbon at the branching point. This branching makes a rigid structure and therefore gives an open space for the thioctic acid moiety (intramolecular S−S part) to immobilize the ligand conjugate to the gold surface. In contrast, the tetravalent type linker's branching parts are flexible enough to allow the large oligosaccharides to move apart and potentially mask the thioctic acid moiety. The ligand conjugate **36** (short spacer, tetravalent) was not able to be effectively immobilized. When a longer spacer arm was inserted (four units of ethylene glycol between the branching part and the thioctic acid moiety), compound **49** could then be successfully immobilized.

CONCLUSION

We have studied the binding of mono- and multivalent oligosaccharide ligands to increasingly complex heparin-binding protein structures. We have devised relatively simple and novel nondestructive methods of conjugation and immobilization that are applicable to a wide range of synthetic or naturally occurring oligosaccharides. The data show that clustering of the biologically active oligosaccharides enhances their affinity for simple

heparin-binding motifs and reduces the impact of surface irregularities or variations in the density of immobilization. For more complex heparin-binding proteins, the density of immobilization and the degree of ligand valency play less of a role. This relative dependence on density can thus be used as one rapid method to characterize the nature of the glycosaminoglycan−protein interaction.

Several technical advantages are conferred by these approaches. The reductive amination technique using an aromatic amino moiety offers a simpler, more quantitatively precise method of conjugation than that reported by Feizi and Chai (*30*). It is suitable for any oligosaccharide with a reducing end and does not require significant modification of their functional sulfate groups. The sulfur−gold immobilization using a thioctic acid moiety permits tighter control of the sulfur reactions, and easier purification of the conjugate. With tri- or tetravalent linkers, the oligosaccharides can easily be incorporated as a clustered form that mimics nature. These novel applications of SPR offer the potential to elucidate a range of fundamental structure−function relations of oligosaccharide−protein interactions at the molecular level and hold promise as a novel approach to rapid throughput screening of new bioactive molecules.

ACKNOWLEDGMENT

We wish to thank Mr. Y. Murakami (Shimazu Co., Kyoto Customer Support Center) for his great support for the measurement of ATR-FT-IR. This work was supported in parts by grants from Japan Science and Technology Agency (YS), the National Institutes of Health (Grants RO1HL39903 and HL079182 to M.S.) and the Department of Veterans Affairs Research Service (to M.S.).

Supporting Information Available: Details of compound syntheses. This material is available free of charge via the Internet at http://pubs.acs.org.

LITERATURE CITED

(1) Varki, A. (1999) In *Essentials of Glycobiology* (Varki, A., Cummings, R., Esko, J., Freeze, H., Hart, G., and Marth, J., Eds.), Cold Spring Harbor Laboratory Press, Cold Spring Harbor, New York, pp 57−68 and references therein.

(2) Gallagher, J. (2001) Heparan sulfate: growth control with a restricted sequence menu. *J. Clin. Invest. 108*, 357−361.

(3) Ostrovsky, O., Berman, B., Gallagher, J., Mulloy, B., Fernig, D. G., Delehedde, M., and Ron, D. (2001) Differential effects of heparin saccharides on the formation of specific fibroblast growth factor (FGF) and FGF receptor complexes. *J. Biol. Chem. 277*, 2444−2453.

(4) Faham, S., Hileman, R. E., Fromm, J. R., Linhardt, R. J., and Rees, D. C. (1996) Heparin structure and interactions with basic fibroblast growth factor. *Science 271*, 1116−1120.

(5) Horan, N., Yan, L., Isobe, H., Whitesides, G. M., and Kahne, D. (1999) Nonstatistical binding of a protein to clustered carbohydrates. *Proc. Natl. Acad. Sci. U.S.A. 96*, 11782−11786.

(6) Houseman, B. T., and Mrksich, M. (2002) Carbohydrate arrays for the evaluation of protein binding and enzymatic modification. *Chem. Biol. 9*, 443−454.

(7) Kato, M., and Mrksich, M. (2004) Using model substrates to study the dependence of focal adhesion formation on the affinity of integrin−ligand complexes. *Biochemistry 43*, 2699−2707.

(8) Fazio, F., Bryan, M. C., Blixt, O., Paulson, J. C., and Wong, C.-H. (2002) Synthesis of sugar arrays in microtiter plate. *J. Am. Chem. Soc. 124*, 14397−14402.

(9) Park, S., Lee, M.-R., Pyo, S.-J., and Shin, I. (2004) Carbohydrate chips for studying high-throughput carbohydrate-protein interactions. *J. Am. Chem. Soc. 126*, 4812−4819.

(10) Plant, A. L., Brigham-Burke, M., Petrella, E. C., and O'Shannessy, D. J. (1995) Phospholipid/alkanethiol bilayers for cell-surface receptor studies by surface plasmon resonance. *Anal. Biochem. 226*, 342−348.

(11) Peterlinz, K. A., and Georgiadis, R. (1996) In situ kinetics of self-assembly by surface plasmon resonance spectroscopy. *Langmuir 12*, 4731−4740.

(12) Liedberg, B., Nylander, C., and Lundström, I. (1983) Surface plasmon resonance for gas detection and biosensing. *Sens. Actuators 4*, 299−304.

(13) Flanagan, M. T., and Pantell, R. H. (1984) Surface plasmon resonance and immunosensors. *Electron. Lett. 20*, 968−970.

(14) Matsubara, K., Kawata, S., and Minami, S. (1988) Optical chemical sensor based on surface plasmon measurement. *Appl. Opt. 27*, 1160−1163.

(15) Suda, Y., Marques, D., Kermode, J. C., Kusumoto, S., and Sobel, M. (1993) Structural characterization of heparins binding domain for human platelets. *Thromb. Res. 69*, 501−508.

(16) Poletti, L. F., Bird, K. E., Marques, D., Harris, R. B., Suda, Y., and Sobel, M. (1997) Structural aspects of heparin responsible for interactions with von Willebrand factor. *Arterioscler., Thromb., Vasc. Biol. 17*, 925−931.

(17) Koshida, S., Suda, Y., Fukui, Y., Ormsby, J., Sobel, M., and Kusumoto, S. (1999) Synthesis of heparin partial structures and their binding activities to platelets. *Tetrahedron Lett. 40*, 5725−5728.

(18) Koshida, S., Suda, Y., Sobel, M., and Kusumoto, S. (2001) Synthesis of oligomeric assemblies of a platelet-binding key disaccharide in heparin and their biological activities. *Tetrahedron Lett. 42*, 1289−1292.

(19) Weis, C. D., and Newkome, G. R. (1990) Building-blocks for cascade polymers. 3. Facile elimination of nitrous-acid form quaternary nitroalkanes. *J. Org. Chem. 55*, 5801−5802.

(20) Ashton, P. R., Boyd, S. E., Brown, C. L., Nepogodiev, S. A., Meijer, E. W., Peerlings, H. W. I., and Stoddart, J. E. (1997) Synthesis of glycodendrimers by modification of poly(propylene imine) dendrimers. *Chem.−Eur. J. 3*, 974−984.

(21) Sobel, M., Soler, D. F., Kermode, J. C., and Harris, R. B. (1992) Localization and characterization of a heparin binding domain peptide of human von Willebrand factor. *J. Biol. Chem. 267*, 8857−886.

(22) Cruz, M. A., Handin, R. I., and Wise, R. J. (1993) The interaction of the von Willebrand factor A1 domain with platelet glycoprotein Ib Ix−The role of glycosylation and disulfide bonding in a monomeric recombinant A1 domain protein. *J. Biol. Chem. 268*, 21238−21245.

(23) Rastegar-Lari, G., Villoutreix, B. O., Ribba, A. S., Legendre, P., Meyer, D., and Baruch, D. (2002) Two clusters of charged residues located in the electropositive face of the von Willebrand factor A1 domain are essential for heparin binding. *Biochemistry 41*, 6668−6678.

(24) Presta, M., Maier, J. A., Rusnati, M., and Ragnotti, G. (1989) Basic fibroblast growth factor is released from endothelial extracellular matrix in a biologically active form. *J. Cell. Physiol. 140*, 68−74.

(25) Koshida, S., Suda, Y., Arano, A., Sobel, M., and Kusumoto, S. (2001) An efficient method for the assembly of sulfated oligosaccharides using reductive animation. *Tetrahedron Lett. 42*, 1293−1296.

(26) Ratner, D. M., Adams, E. W., Su, J., O'Keefe, B. R., Mrksich, M., and Seeberger, P. H. (2004) Probing protein−carbohydrate interactions with microarrays of synthetic oligosaccharides. *ChemBioChem 5*, 379−383.

(27) Suda, Y., Kusumoto, S., and Arano, A. (2003) Japan Patent P2003-83969A.

(28) Karamanska, R., Mukhopadyay, B., Russell, D. A., and Field, R.A. (2005) Thioctic acid amides: convenient tethers for achieving low nonspecific protein binding to carbohydrates presented on gold surfaces. *Chem. Commun.* 3334−3336.

(29) de Paz, J. L., Noti, C., and Seeberger, P. H. (2006) Microarrays of synthetic heparin oligosaccharides. *J. Am. Chem. Soc. 128*, 2766−2767.

(30) Feizi, T., and Chai, W. (2004) Oligosaccharide microarrays to decipher the glyco code. *Nat. Rev. 5*, 582−588.

BC0600620

Journal of Neurochemistry, 2006, **99**, 198–205 doi:10.1111/j.1471-4159.2006.04035.x

Styrylbenzoazole derivatives for imaging of prion plaques and treatment of transmissible spongiform encephalopathies

Kensuke Ishikawa,* Yukitsuka Kudo,† Noriyuki Nishida,‡ Takahiro Suemoto,§ Tohru Sawada,§ Toru Iwaki¶ and Katsumi Doh-ura*

**Department of Prion Research, Tohoku University Graduate School of Medicine, Sendai, Japan*

†Division of Telecommunication and Information Technology, Biomedical Engineering Research Organization, Tohoku University, Sendai, Japan

‡Division of Cellular and Molecular Biology, Nagasaki University Graduate School of Biomedical Sciences, Nagasaki, Japan

§BF Research Institute Inc., Osaka, Japan

¶Department of Neuropathology, Graduate School of Medical Sciences, Kyushu University, Fukuoka, Japan

Abstract

Recent prevalence of acquired forms of transmissible spongiform encephalopathies (TSEs) has urged the development of early diagnostic measures as well as therapeutic interventions. To extend our previous findings on the value of amyloid imaging probes for these purposes, styrylbenzoazole derivatives with better permeability of blood–brain barrier (BBB) were developed and analyzed in this study. The new styrylbenzoazole compounds clearly labeled prion protein (PrP) plaques in brain specimens from human TSE in a manner irrespective of pathogen strain, and a representative compound BF-168 detected abnormal PrP aggregates in the brain of TSE-infected mice when the probe was injected intravenously. On the other hand, most of the compounds inhibited abnormal PrP formation in TSE-infected cells with IC_{50} values in the nanomolar range, indicating that they represent one of the most potent classes of inhibitor ever reported. BF-168 prolonged the lives of mice infected intracerebrally with TSE when the compound was given intravenously at the preclinical stage. The new compounds, however, failed to detect synaptic PrP deposition and to show pathogen-independent therapeutic efficacy, similar to the amyloid imaging probes we previously reported. The compounds were BBB permeable and non-toxic at doses for imaging and treatment; therefore, they are expected to be of practical use in human TSE.

Keywords: amyloid imaging, anti-prion activity, pathogen strain, prion disease, styrylbenzoazole derivatives.

J. Neurochem. (2006) **99**, 198–205.

The transmissible spongiform encephalopathies (TSEs) or prion diseases form a group of neurodegenerative disorders characterized by abnormal deposition of protease-resistant isoforms of prion protein (PrP) in the CNS (Prusiner 1991). TSEs are classified as sporadic, hereditary or environmentally acquired, and have become a serious public health issue because of the recent prevalence of acquired Creutzfeldt–Jakob disease (CJD), such as the variant form due to bovine spongiform encephalopathy (Will *et al.* 1996) and the iatrogenic form with cadaveric growth hormone or dura grafts (Brown *et al.* 2000). There is an urgent need to develop prophylactic and therapeutic interventions as well as diagnostic measures at the preclinical or early clinical stages of these incurable diseases.

We have previously reported that some amyloid imaging compounds, primarily derived from amyloid dyes such as

Received February 16, 2006; revised manuscript received May 25, 2006; accepted May 30, 2006.

Address correspondence and reprint requests to Dr Kensuke Ishikawa, Division of Prion Biology, Department of Prion Research, Tohoku University Graduate School of Medicine, 2–1 Seiryo-machi, Aoba-ku, Sendai 980-8575, Japan. E-mail: ishikawa@mail.tains.tohoku.ac.jp

Abbreviations used: AD, Alzheimer's disease; BBB, blood–brain barrier; BSB, (trans, trans)-1-bromo-2,5-bis-(3-hydroxycarbonyl-4-hydroxy)styrylbenzene; CJD, Creutzfeldt–Jakob disease; DMSO, dimethylsulfoxide; FDDNP, 2-(1-[6-[(2-fluoroethyl)(methyl)amino]-2-naphthyl]ethylidene)malononitrile; GSS, Gerstmann–Strässler–Scheinker syndrome; ICR, Institute of Cancer Research; ID, injected dose; NT, not tested; PrP, prion protein; PrPres, protease-resistant PrP; PTA, phosphotungstic acid; PVDF, polyvinylidene difluoride; TSE, transmissible spongiform encephalopathy.

Congo red and thioflavin T, are useful for detection of prion plaques and treatment of TSE (Ishikawa *et al.* 2004). These compounds, however, are limited in their ability because of inefficient brain uptake. Here we describe new compounds, styrylbenzoazole derivatives, which have been developed for practical use and analyzed for their PrP imaging ability, anti-prion activity, therapeutic efficacy, brain uptake and toxicity.

Materials and methods

Chemicals and experimental models

All of the test compounds were synthesized at Tanabe R & D (Saitama, Japan) and used freshly after being dissolved in 100% dimethylsulfoxide (DMSO).

Cultured cells were grown in Opti-MEM (Invitrogen, Carlsbad, CA, USA) supplemented with 10% fetal calf serum. As cellular models of TSE, we used mouse neuroblastoma (N2a) cells persistently infected with the RML strain (ScN2a) (Race *et al.* 1988) and six other prion-infected cell lines: N2a58 cells individually infected with the RML strain, the 22L strain (Nishida *et al.* 2000) and Fukuoka-1 strain (Ishikawa *et al.* 2004); N2a cells infected with the 22L strain; mouse hypothalamic cells (GT1-7) infected with the 22L strain (Milhavet *et al.* 2000); and mouse fibroblast cells (L929) infected with the RML strain (Vorberg *et al.* 2004).

Tg7 mice overexpressing hamster PrP (Race *et al.* 1995) and Tga20 mice overexpressing mouse PrP (Fischer *et al.* 1996) were also used. These mouse models were intracerebrally infected with 20 μL brain homogenate comprising 1% (w/v) of the 263K strain and the RML strain respectively. The Tg7 mice showed plaque-type PrP deposition between the cerebral cortex and hippocampus by 6 weeks after infection, followed by synaptic-type PrP deposition in the thalamus. The Tga20 mice showed similar pathological deposition, but plaques were not seen as frequently. Each mouse weighed ~30 g, and was maintained under deep ether anesthesia for minimum distress during all surgical procedures. Permission for the animal study was obtained from either the Animal Experiment Committee of Kyushu University or Tohoku University, Japan.

Brain uptake study

Test compounds were administered intravenously to Institute of Cancer Research (ICR) mice under ether anesthesia to determine initial brain uptakes. At 2 or 30 min after injection, the brains were removed, weighed and homogenized with saline. After centrifugation of the homogenate at 21 900 *g* for 10 min, the supernatant was applied to a conditioned C18 solid-phase extraction cartridge, and the compounds were eluted with methyl alcohol. Fluorescence was detected by high performance liquid chromatography with a fluorescence detector as reported previously (Okamura *et al.* 2005), and the percentage of injected dose per gram (%ID/g) was used as a measure of the level of the compounds in the brain.

In vitro PrP imaging in sections

Autopsy-diagnosed brain samples from cases of Gerstmann–Strässler–Scheinker syndrome (GSS) ($n = 2$), sporadic CJD ($n = 5$), iatrogenic dura CJD with synaptic PrP deposition ($n = 1$) and non-TSE control cases with amyloid lesions [Alzheimer's disease (AD), $n = 2$] or without amyloid lesions (cerebral infarction, $n = 1$) were obtained from the Department of Neuropathology, Kyushu University, Japan. After fixation in 10% buffered formalin for 2 weeks, each sample of TSE was immersed in 98% formic acid for the reduction of prion infectivity, embedded in paraffin and cut into sections 7 μm thick. Sections of a variant CJD case were kindly provided by Dr James W. Ironside of the CJD Surveillance Unit, Edinburgh, UK. For neuropathological staining, deparaffinized sections were immersed in 1% Sudan black solution to quench tissue autofluorescence. They were then incubated for 30 min in 1-μM solutions of the test compounds, rinsed with distilled water and examined under a fluorescence microscope (DMRXA; Leica Instruments, Wetzler, Germany) with a UV or FITC filter set.

For comparison, each section was subsequently immunoassayed for PrP as described previously (Doh-ura *et al.* 2000). Briefly, the sections were treated with a hydrolytic autoclave and incubated with a rabbit primary antibody, c-PrP, which was raised against a mouse PrP fragment, amino acids 214–228 (1 : 200; Immuno-Biological Laboratories, Gunma, Japan), followed by incubation with a horseradish peroxidase-conjugated secondary antibody (1 : 200; Vector Laboratories, Burlingame, CA, USA). The reaction product was developed with 3,3′-diaminobenzidine tetrahydrochloride solution and counterstained with hematoxylin. Paraffin-embedded brains of experimental animals were similarly investigated.

In vivo PrP imaging in model animals

BF-168 (molecular weight 312.34) dissolved in 10% DMSO was administered intravenously (0.5–5 mg/kg body weight) into Tg7 mice at 6–7 weeks after injection when the mice showed no apparent clinical signs of TSE. As controls, vehicle alone was similarly injected into infected mice, and BF-168 was administered into uninfected mice. The animals were killed at various time points, and the brains were rapidly frozen and cut into coronal sections 10 μm thick using a cryostat (CM3050; Leica Instruments). The sections were thaw-mounted on slides, dried and coverslipped. They were examined under a fluorescence microscope and further analyzed immunohistochemically as described above.

In vitro treatment in cell cultures

Abnormal PrP formation was assayed by the content of protease-resistant PrP (PrPres) in cellular models of TSE as described previously (Caughey and Raymond 1993). Each compound was added at the designated concentrations when cells were passaged at 10% confluence, while maintaining the final concentration of DMSO in the medium at < 0.5%. The cells were allowed to grow to confluence and lysed with lysis buffer (0.5% sodium deoxycholate, 0.5% Nonidet P-40, phosphate-buffered saline). For analysis of PrPres, samples were digested with 10 μg/mL proteinase K for 30 min, and the digestion was stopped with 0.5 mM phenylmethylsulfonyl fluoride. The samples were centrifuged at 100 000 *g* for 30 min, and pellets were resuspended in 1 × sample loading buffer and boiled. For analysis of cellular PrP in N2a cells, cell lysates were mixed directly with a quarter volume of 5 × sample loading buffer and boiled. These samples were separated by electrophoresis on a 15% Tris–glycine–sodium dodecyl sulfate polyacrylamide gel and electroblotted on to a polyvinylidene difluoride (PVDF) filter (Millipore, Bedford, MA, USA). PrP was detected using a monoclonal antibody, SAF83 (1 : 5000; SPI-BIO, Massy, France), followed by an alkaline phosphatase-conjugated

goat anti-mouse antibody (1 : 20 000; Promega, Madison, WI, USA). Immunoreactive blots were visualized with CDP-Star detection reagent (Amersham, Piscataway, NJ, USA). More than two independent assays were performed in each experiment and signals were analyzed using image analysis software. The approximate concentration of the compound giving 50% inhibition of PrPres formation, relative to the vehicle-treated control (IC_{50}), was estimated by signal intensity. To control for the detection limits of western blotting, we performed additional experiments utilizing sodium phosphotungstic acid (PTA) precipitation, which is the most sensitive technique presently available to detect PrPres (Safar *et al.* 1998). The PTA precipitation was undertaken on cell lysates of ScN2a treated with BF-168 at a designated concentration. The resulting pellets were collected by centrifugation and then analyzed by immunoblotting as described above.

In vivo treatment in model animals

BF-168 solution (4 mg/kg body weight) or vehicle alone was injected intravenously to experimental animals ($n = 5$) once a week. The treatment was started at 2 weeks after injection for Tg7 mice and at 4 weeks after injection for Tga20 mice, and repeated for 4 weeks. A continuous subcutaneous infusion of BF-168 was also given to Tga20 mice ($n = 5$) using an Alzet osmotic pump (Durect, Cupertino, CA, USA). In accordance with the manufacturer's instructions, each pump was filled with BF-168 solution at the designated doses and placed in a subcutaneous area of the back at 4 weeks after injection. The animals showed no apparent adverse effects of the treatment and were monitored 5 days a week until obvious clinical signs appeared. Statistical significance was analyzed by one-way ANOVA followed by Scheffé's method for multiple comparisons.

Results

Brain uptake and toxicity

We designed and synthesized novel styrylbenzoxazole derivatives (Table 1), styrylbenzothiazole and styrylbenzoimidazole derivatives (Table 2) with more efficient permeability of the BBB and less toxicity. Values for brain uptake at 2 min after intravenous injection of the compounds were in the 2.4–17.0%ID/g range, indicating a satisfactory level for imaging probes. Their washouts from the brain varied, with the ratio of %ID/g at 2 min to that at 30 min after injection ranging from 1.0 to 56.9. Acute toxicity was tested by administering each compound intravenously at ~10 mg/kg body weight into normal ICR mice. No apparent toxic effect was observed with any of the compounds tested.

PrP imaging ability

Imaging of abnormal PrP deposition by the compounds was first performed in brain sections of human TSE. The compounds fluorescently labeled most of the PrP plaques in cerebellar cortices of both GSS cases (Fig. 1a, representative data). Among sections from the sporadic CJD cases, PrP deposition was labeled only in a case with plaques (Fig. 1c). In the cerebral cortex from the variant CJD case, large core plaques were detectable, whereas the majority of immunopositive aggregates were not labeled (Fig. 1e). In contrast, no fluorescence signal was identified in sections from the dura CJD case or the other sporadic CJD cases that

Table1 Chemical structure, PrPres inhibition and brain uptake of styrylbenzoxazole derivatives including BF-168

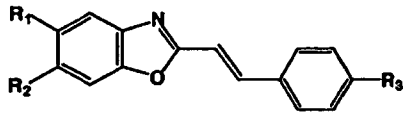

Compound	R_1	R_2	R_3	IC_{50} (nM)[a]	Brain uptake (%ID/g)[b] 2 min	Brain uptake (%ID/g)[b] 30 min	Ratio of 2 to 30 min brain uptake
BF-168	H	$O(CH_2)_2F$	$NH(CH_3)$	0.4	3.9[c]	1.6	2.4
BF-125	H	H	$N(C_2H_5)_2$	10.2	3.0	3.0	1.0
BF-133	F	H	$N(CH_3)_2$	1.6	5.5	3.8	1.4
BF-135	NO_2	H	$N(CH_3)_2$	< 1	NT[d]	NT	-
BF-140	F	H	NH2	< 1	5.5	1.1	5.0
BF-145	F	H	$NH(CH_3)$	< 1	4.4	1.6	2.8
BF-148	H	F	$N(CH_3)_2$	< 1	NT	NT	-
BF-165	H	H	$NH(CH_3)$	7.1	7.2	NT	-
BF-169	H	OH	$NH(CH_3)$	2.4	NT	NT	-
BF-173	I	H	NH_2	2.2	NT	NT	-
BF-180	I	H	$NH(CH_3)$	8.5	2.4	1.8	1.3
BF-191	H	H	Cl	1.8	12.0	1.7	7.1
BF-208	H	H	F	< 1	11.0	0.53	20.8
N-282	H	H	$N(CH_3)_2$	2.1	4.0	1.7	2.4
N-407	H	H	H	< 1	17.0	0.99	17.2

[a]IC_{50}, approximate concentration of a compound giving 50% inhibition of PrPres formation relative to the control in ScN2a cells.
[b]%ID/g, percentage of injected dose per gram in the brains of normal mice.
[c]already reported in the previous work (Okamura *et al.*, 2004).
[d]NT, not tested.

Table 2 Chemical structure, PrPres inhibition and brain uptake of styrylbenzothiazole and styrylbenzoimidazole derivatives

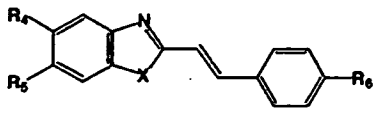

Compound	X	R_4	R_5	R_6	IC_{50} (nM)[a]	Brain uptake (%ID/g)[b] 2 min	Brain uptake (%ID/g)[b] 30 min	Ratio of 2 to 30min brain uptake
BF-124	S	H	H	$N(C_2H_5)_2$	18.1	2.4	2.5	1.0
BF-162	S	F	H	$N(CH_3)_2$	1.4	NT[c]	NT	-
N-276	S	H	H	$N(CH_3)_2$	< 1	NT	NT	-
N-438	S	H	H	H	< 1	11.0	2.0	5.5
BF-126	NH	H	H	$N(C_2H_5)_2$	21	7.2	0.16	45
BF-166	NH	F	H	$N(C_2H_5)_2$	1.1	NT	NT	-
N-457	NH	H	H	Cl	< 1	7.1	0.21	33.8
N-491	NH	H	H	H	1.9	7.4	0.13	56.9

[a]IC_{50}, approximate concentration of a compound giving 50% inhibition of PrPres formation relative to the control in ScN2a cells.
[b]%ID/g, percentage of injected dose per gram in the brains of normal mice.
[c]NT, not tested.

included perivacuolar and/or synaptic PrP deposition (data not shown). Background staining was barely observed after rinsing off the excess compound. Immunohistochemical analysis of PrP revealed that the compounds achieved high-specificity labeling (Figs 1b, d and f). The compounds displayed no signal in control sections without amyloid lesions (data not shown).

Similar results were observed in experimental mice. PrP plaques were specifically labeled in brain sections of Tg7 mice infected with the 263K strain, and there was no PrP immunopositive reaction or fluorescence signal in brain sections of uninfected mice (data not shown). We performed *in vivo* experiments using presymptomatic Tg7 mice at a later stage of TSE. A typical image is shown in Fig. 1(g); peripheral administration of BF-168 fluorescently labeled plaques in the cerebral white matter, indicating that the compound efficiently entered the brain and bound to coarse PrP deposits. Subsequent immunostaining verified the specificity and sensitivity for PrP (Fig. 1h). Non-specific staining, such as cerebrovascular labeling, was occasionally observed at 4 h after injection of 5 mg/kg BF-168, but not after 8 h or more. The stability of the fluorescence signals was examined at various time points up to 24 h after injection and the dye–PrP complex remained visible at the latest time. In contrast, there was no significant labeling after an injection of BF-168 into uninfected animals, or after an injection of vehicle alone to terminally ill Tg7 mice. Similar results were obtained for Tga20 mice infected with the RML strain, although plaques were less frequently detected (data not shown).

Anti-prion activity *in vitro*

The anti-prion activities of the compounds were investigated using ScN2a cells, which are most commonly used for drug screening for TSE treatment. Styrylbenzoxazole derivatives, including BF-168, were evaluated and confirmed to inhibit PrPres formation with IC_{50} values in the nanomolar or subnanomolar range (Fig. 2a and Table 1). Styrylbenzothiazole and styrylbenzoimidazole derivatives were similarly potent, in a dose-dependent manner, within a non-toxic dose range (~10 μM) (Table 2). Treatment with vehicle alone showed no inhibitory effect compared with untreated controls (Fig. 2a). We utilized PTA precipitation, which increases the sensitivity of western blotting, and confirmed the potency of BF-168 at a concentration of 10 times the IC_{50}. Furthermore, radiographic film was exposed to the blotted PVDF membranes for 10 times longer than usual before developing. No significant signals were visualized, whereas bands representing the vehicle-treated control were so strong as to be already saturated (Fig. 2b). To determine whether the efficacy was transient, ScN2a cells treated with 10 nM BF-168 were further cultured for 2 weeks in the absence of BF-168. PrPres signals never reappeared, even through four passages after discontinuation of the treatment (Fig. 2c). To exclude the possibility of interference with immunodetection, BF-168 solution at a final concentration of 10 nM was added to a lysate of untreated ScN2a cells before proteinase K digestion. PrP signals were not affected (data not shown). Nor was any alteration observed in cellular PrP level of N2a cells after treatment with 10 nM BF-168 (Fig. 2d).

To investigate whether the efficacy of the compounds depends on pathogen strain, we tested BF-168 in three N2a58 cell lines individually infected with different strains. As shown in Table 3, BF-168 was only effective in N2a58 cells infected with the RML strain, although the inhibitory activity was not as strong as in ScN2a cells (~1 μM). In contrast, BF-168 was ineffective in the same N2a58 cells infected with the 22L or Fukuoka-1 strains up to 10 μM, a dose at which the compound showed host cytotoxicity.

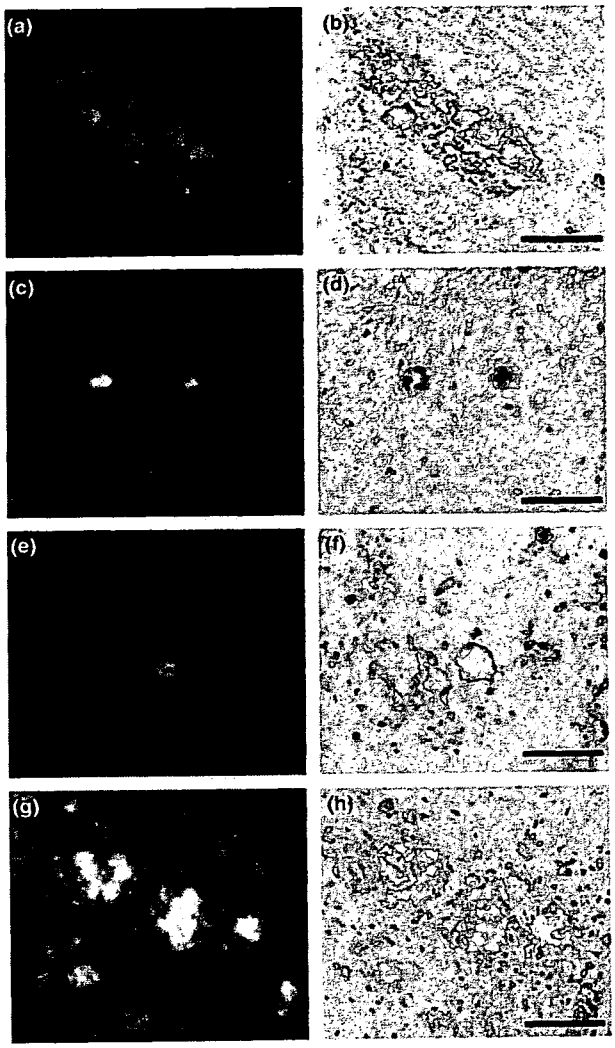

Fig. 1 PrP imaging *in vitro* and *in vivo*. BF-168 fluorescently labeled PrP deposition in a cerebellar section from the case of GSS (a), and in cerebral sections from cases of sporadic CJD with plaques (c) and variant CJD (e). Similar results were obtained from the brains of living TSE-infected mice that were intravenously injected with BF-168 solution (0.5 mg/kg). BF-168 detected PrP deposition in the cerebral white matter between the cortex and hippocampus (g). Sections (a, c, e and g) were subsequently immunoassayed for PrP (b, d, f and h). Bars represent 100 μm (a–f) and 25 μm (g and h).

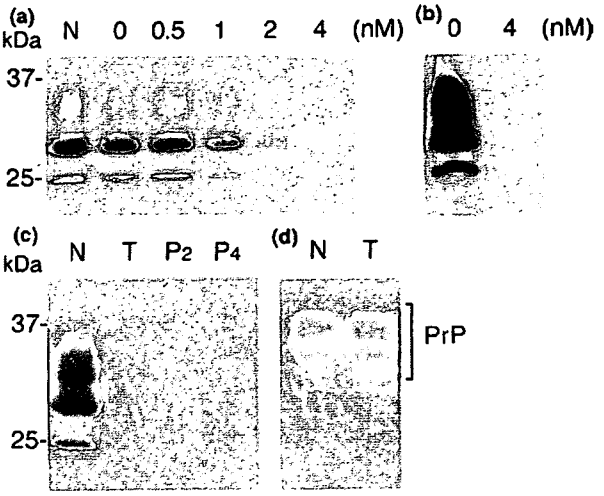

Fig. 2 Effects of BF-168 on PrP expression in ScN2a and N2a cells. BF-168 was added at the designated concentrations to freshly passaged cells. PrPres formation in ScN2a cells was inhibited in a dose-dependent manner (a). To exclude the sensitivity limit of immunoblotting, ScN2a cells treated with 4 nM BF-168 were also analyzed by sodium PTA, and no significant signals were visualized (b). ScN2a cells treated with 10 nM BF-168 were maintained for an additional four passages, and the PrPres signal was not restored in the absence of BF-168 (c). PrP expression was not affected in N2a cells that were grown in the presence of 10 nM BF-168 (d). Lane N, untreated cells; lane 0, cells treated with vehicle alone; lane T, cells treated with 10 nM BF-168; lanes P_2 and P_4, cells following two and four passages after treatment respectively. Bars on the left indicate molecular size markers at 37 and 25 kDa.

Table 3 Anti-prion activities (IC_{50}) of BF-168 in various types of TSE-infected cells

Host cells	Pathogen strains		
	RML	22L	Fukuoka-1
N2a	0.4 nM	None[a]	-[b]
N2a58	~1 μM	None	None
L929	~10 nM	-	-
GT1-7	-	None	-

[a]None, no significant PrPres inhibition up to 10 μM, a dose that affect the rate of cell growth.
[b], not available.

Furthermore, we established L929 cells stably infected with the RML strain. BF-168 inhibited PrPres formation in the RML-infected L929 cells with an IC_{50} in the nanomolar range. We also tested potency against the 22L strain in two other cell lines, N2a and GT1-7 cells. BF-168 was ineffective in either cell line infected with the 22L strain. Other compounds tested here demonstrated similar results (data not shown). These results suggest that the styrylbenzoxazole derivatives exert their inhibitory activity on PrPres formation in a strain-dependent, but not a host cell-dependent, manner.

Therapeutic efficacy *in vivo*

The therapeutic activity of the compounds *in vivo* was assayed in two different mouse models using BF-168 as a representative. Treatment was initiated 2–4 weeks after TSE infection and repeated once a week for 4 weeks. The dosage at a single administration corresponded to a dose sufficient to detect PrP plaques. As shown in Table 4, there was no

Table 4 Effects of BF-168 treatment on intracerebrally TSE-infected mice

Mouse - pathogen strain	n	Dose (mg/kg/week)	Administration	Incubation period Mean ± SD (days)
Tg7 - 263K				
	7	Control	-	49.4 ± 1.9
	5	Vehicle	i.v.[a]	50.2 ± 4.1
	5	4	i.v.	52.2 ± 2.6
Tga20 - RML				
	7	Control	-	66.6 ± 1.6
	5	Vehicle	i.v.	64.8 ± 1.6
	5	4	i.v.	72.2 ± 2.5*
	5	10	s.c.[b]	66.0 ± 3.1

* $p < 0.001$ versus the oher groups.

[a]i.V., intravenous injection of BF-168 once a week for 4 weeks from 2 weeks p.i. for Tg7, or 4 weeks p.i. for Tga20.

[b]s.c., continous subcutaneous infusion of BF-168 for 4 weeks from 4 weeks p.i.

significant difference in incubation periods between groups of Tg7 mice infected intracerebrally with the 263K strain, with or without treatment. In contrast, intravenous injection with 4 mg/kg BF-168 significantly prolonged the incubation period (~ 11.4%) of Tga20 mice intracerebrally infected with the RML strain.

In another trial, we used osmotic pumps filled with BF-168 solution, assuming that the route of administration is a key issue. The pump worked continuously for 4 weeks, and the total dosage for the duration was selected to correspond to two to three times that administered intravenously. Subcutaneous infusion of BF-168, however, did not prolong incubation periods of Tga20 mice intracerebrally infected with the RML strain (Table 4). There was no significant difference in incubation period in either group of infected mice between untreated controls and controls treated with vehicle alone.

Discussion

Our results show that styrylbenzoazole derivatives represent candidates for imaging probes as well as therapeutic drugs for TSE. It has been increasingly necessary to develop minimally non-invasive methods for recognizing early clinical infection and evaluating treatment of TSE. We have already focused on two β-amyloid imaging probes and reported them as potential agents for TSE (Ishikawa *et al.* 2004). The problem is, however, that they seemed to have practical limitations because of inadequate brain uptake and washout. Here, we confirmed that novel styrylbenzoazole derivatives clearly labeled PrP plaques *in vitro* and BF-168, the parent compound, entered the brain and labeled PrP plaques *in vivo*, even at a 20-fold lower dose than the probes we previously reported. In brain uptake studies, all of the compounds showed BBB permeability with >1%ID/g, which is proposed to be sufficient for neuroimaging probes. The background staining of 0.5 mg/kg BF-168 was almost absent at 4 h after administration, suggesting excellent clearance from the brain.

Most of styrylbenzoazole derivatives labeled β-amyloid aggregates in AD specimens in this study (data not shown) as well as in the previous study on Alzheimer's (Okamura *et al.* 2004). This is also observed with 2-(1-[6-[(2-fluoroethyl)(methyl)amino]-2-naphthyl]ethylidene)malononitrile (FDDNP), one of the promising agents for imaging β-amyloid deposition. FDDNP has been reported to label PrP plaques in brain sections, and is a candidate for imaging PrP deposition (Bresjanac *et al.* 2003). These findings imply lack of disease specificity, but the compounds should still be useful for some types of TSE, because anatomical distributions of amyloid deposition are characteristically different between diseases. Pathological changes including amyloid deposition of AD brain are always observed in the hippocampus but not in the cerebellum, whereas those of TSE tend to be absent from the hippocampus but to be demonstrated in the cerebellum.

Styrylbenzoazole derivatives detected predominantly PrP plaques, especially in specimens of sporadic CJD with plaques and variant CJD. However, their ability to detect synaptic or perivacuolar PrP deposition remains inconclusive, until more sensitive investigations, such as autoradiography, are available. The compounds tested in this study can be used with radionuclides. ^{18}F-radiolabeled BF-168, which has already been employed for labeling of β-amyloid deposits including both neuritic and diffuse plaques in AD brain (Okamura *et al.* 2004), may be a suitable tool for investigating whether PrP deposition, other than plaque type, can be detected.

This study demonstrated that styrylbenzoazole derivatives have more potent anti-prion activity than the amyloid imaging probes reported previously (Ishikawa *et al.* 2004). Although the neuropathological processes remain unclear, one of the most likely strategies for TSE treatment is a small-molecule drug that can enter the brain and inhibit abnormal PrP formation. It is important to emphasize that styrylbenzoazole derivatives have a wide concentration safety margin, and some were effective even at subnanomolar doses in ScN2a cells. Dozens of drug candidates for TSE have been reported to date but, as far as we know, the most potent inhibitor class for abnormal PrP formation in ScN2a cells is specific blocking antibodies with an IC_{50} in the nanomolar range (Peretz *et al.* 2001).

BF-168 showed no apparent alteration in cellular PrP expression level in N2a cells, and also labeled abnormal PrP deposition both *in vitro* and *in vivo*. These data suggest that styrylbenzoazole derivatives might interact directly with abnormal PrP molecules to block the conversion of normal to abnormal PrP. The structure–activity relationship, examined by introducing side-chain or functional groups into the benzoazole and/or benzene rings, demonstrates that the inhibitory potency is not always the same, even among

closely related compounds (data not shown). Although we could not obtain any insight into inhibitory mechanisms, the efficacy of BF-168 was dependent on pathogen strain, and this is consistent with our previous work using three types of cell lines (Ishikawa *et al.* 2004). In an attempt to further explore strain dependency, we tested three different pathogen strains in one host cell line, and three different host cell lines with one pathogen strain. BF-168 inhibited abnormal PrP formation in all three types of RML-infected cells, including ScN2a cells. By contrast, BF-168 did not demonstrate any inhibitory activity in the 22L- or Fukuoka-1-infected cells. It is well known that prion strains differ in their biological profiles such as the degree of glycosylation and the conformation of PrP molecules. In the imaging experiments we confirmed that the compound bound to a certain type of abnormal PrP aggregates. Thus, it was assumed that the therapeutic efficacy might be based on blocking certain interactions between normal and abnormal PrP, and that BF-168 might recognize the PrP conformation. However, considering a discrepancy in the *in vivo* experiment between PrP imaging and treatment using infected Tg7 mice, these inferences remain unsupported and the precise mechanism of the strain-dependent efficacies needs to be elucidated.

Kocisko *et al.* (2004) reported that anti-prion activity *in vitro* does not always correlate with that *in vivo*. With *in vivo* testing, there are many variables, such as inoculation route, dosing protocol and pathogen strain. The efficacy differed according to the BF-168 administration route in Tga20 mice, even though the dose administered subcutaneously for the same duration was no less than that administered intravenously. This might be due to differences in stability and clearance of BF-168 in relation to the route of administration.

Most previous therapeutic investigations showed a significant benefit *in vivo* when the treatment was started before, or soon after, peripheral TSE infection. Although the efficacy of BF-168 was limited, it is noteworthy that we obtained significant results with peripheral administration at a later stage of the intracerebral infection. In addition, BF-168 showed excellent brain uptake and binding affinity towards PrP aggregates *in vivo*, even at a low dose, suggesting that the compound should be a good imaging probe for clinical use. In the treatment of infected Tga20 mice, BF-168 showed almost the same prolongation of the incubation period but with a 10-fold smaller dose than (trans, trans)-1-bromo-2,5-bis-(3-hydroxycarbonyl-4-hydroxy)styrylbenzene (BSB), which we reported previously as one of the amyloid imaging probes applicable for TSE (Ishikawa *et al.* 2004). BF-168 showed a low IC_{50} of 0.4 nM in treatment of ScN2a cells, whereas the IC_{50} of BSB was more than 1000-fold higher (1.4 μM). We decided the dosing protocol for our experimental animals from *in vitro* data, including the ratio of these IC_{50} values, and from an *invivo* imaging experiment in which 0.1 mg BF-168 per injection was enough to detect PrP deposition. It is also necessary to consider washout of the compound from the brain. Further studies are required to examine issues such as dose–response relationships, administration time and dosing conditions. Furthermore, there was a problem in that administration frequency was limited because animal tail tissue was damaged by repetitive intravenous injections. In addition, it should be investigated whether compounds with slower washout from the brain are more suitable as therapeutic agents.

In conclusion, styrylbenzoazole derivatives efficiently entered the brain and labeled pathological PrP deposition, and demonstrated some anti-prion activities both *in vitro* and *in vivo*. Although their efficacy depended on the pathogen strain, these are a new class of compounds with potential as therapeutic drugs and imaging probes for TSE.

Acknowledgements

This study was supported by grants to KD from the Ministry of Health, Labour and Welfare (H16-kokoro-024) and the Ministry of Education, Culture, Sports, Science and Technology 13557118, 14021085, Japan. The authors thank Dr James W. Ironside of the CJD Surveillance Unit, Edinburgh, UK, for providing the variant CJD specimens.

References

Bresjanac M., Smid L. M., Vovko T. D., Petric A., Barrio J. R. and Popovic M. (2003) Molecular-imaging probe 2-(1-[6-[(2-fluoroethyl)(methyl) amino]-2-naphthyl]ethylidene) malononitrile labels prion plaques *in vitro*. *J. Neurosci.* **23**, 8029–8033.

Brown P., Preece M., Brandel J. P. *et al.* (2000) Iatrogenic Creutzfeldt–Jakob disease at the millennium. *Neurology* **55**, 1075–1081.

Caughey B. and Raymond G. J. (1993) Sulfated polyanion inhibition of scrapie-associated PrP accumulation in cultured cells. *J. Virol.* **67**, 643–650.

Doh-ura K., Mekada E., Ogomori K. and Iwaki T. (2000) Enhanced CD9 expression in the mouse and human brains infected with transmissible spongiform encephalopathies. *J. Neuropathol. Exp. Neurol.* **59**, 774–785.

Fischer M., Rulicke T., Raeber A., Sailer A., Moser M., Oesch B., Brandner S., Aguzzi A. and Weissmann C. (1996) Prion protein (PrP) with amino-proximal deletions restoring susceptibility of PrP knockout mice to scrapie. *EMBO J.* **15**, 1255–1264.

Ishikawa K., Doh-ura K., Kudo Y., Nishida N., Murakami-Kubo I., Ando Y., Sawada T. and Iwaki T. (2004) Amyloid imaging probes are useful for detection of prion plaques and treatment of transmissible spongiform encephalopathies. *J. Gen. Virol.* **85**, 1785–1790.

Kocisko D. A., Morrey J. D., Race R. E., Chen J. and Caughey B. (2004) Evaluation of new cell culture inhibitors of protease-resistant prion protein against scrapie infection in mice. *J. Gen. Virol.* **85**, 2479–2483.

Milhavet O., McMahon H. E., Rachidi W. *et al.* (2000) Prion infection impairs the cellular response to oxidative stress. *Proc. Natl Acad. Sci. USA* **97**, 13 937–13 942.

Nishida N., Harris D. A., Vilette D., Laude H., Frobert Y., Grassi J., Casanova D., Milhavet O. and Lehmann S. (2000) Successful transmission of three mouse-adapted scrapie strains to murine neuroblastoma cell lines overexpressing wild-type mouse prion protein. *J. Virol.* **74**, 320–325.

Okamura N., Suemoto T., Shimadzu H. *et al.* (2004) Styrylbenzoxazole derivatives for *in vivo* imaging of amyloid plaques in the brain. *J. Neurosci.* **24**, 2535–2541.

Okamura N., Suemoto T., Furumoto S. *et al.* (2005) Quinoline and benzimidazole derivatives: candidate probes for *in vivo* imaging of tau pathology in Alzheimer's disease. *J. Neurosci.* **25**, 10 857–10 862.

Peretz D., Williamson R. A., Kaneko K. *et al.* (2001) Antibodies inhibit prion propagation and clear cell cultures of prion infectivity. *Nature* **412**, 739–743.

Prusiner S. B. (1991) Molecular biology of prion diseases. *Science* **252**, 1515–1522.

Race R. E., Caughey B., Graham K., Ernst D. and Chesebro B. (1988) Analyses of frequency of infection, specific infectivity, and prion protein biosynthesis in scrapie-infected neuroblastoma cell clones. *J. Virol.* **62**, 2845–2849.

Race R. E., Priola S. A., Bessen R. A., Ernst D., Dockter J., Rall G. F., Mucke L., Chesebro B. and Oldstone M. B. (1995) Neuron-specific expression of a hamster prion protein minigene in transgenic mice induces susceptibility to hamster scrapie agent. *Neuron* **15**, 1183–1191.

Safar J., Wille H., Itri V., Groth D., Serban H., Torchia M., Cohen F. E. and Prusiner S. B. (1998) Eight prion strains have PrP(Sc) molecules with different conformations. *Nat. Med.* **4**, 1157–1165.

Vorberg I., Raines A., Story B. and Priola S. A. (2004) Susceptibility of common fibroblast cell lines to transmissible spongiform encephalopathy agents. *J. Infect. Dis.* **189**, 431–439.

Will R. G., Ironside J. W., Zeidler M. *et al.* (1996) A new variant of Creutzfeldt–Jakob disease in the UK. *Lancet* **347**, 921–925.

Surface Plasmon Resonance Analysis for the Screening of Anti-prion Compounds

Satoshi KAWATAKE,[a] Yuki NISHIMURA,[a] Suehiro SAKAGUCHI,[b] Toru IWAKI,[c] and Katsumi DOH-URA*,[a]

[a] *Department of Prion Research, Tohoku University; Sendai 980–8575, Japan:* [b] *Department of Molecular Microbiology and Immunology, Nagasaki University; Nagasaki 852–8523, Japan: and* [c] *Department of Neuropathology, Neurological Institute, Kyushu University; Fukuoka 812–8582, Japan.*

Received November 2, 2005; accepted January 24, 2006; published online January 27, 2006

The interaction of anti-prion compounds and amyloid binding dyes with a carboxy-terminal domain of prion protein (PrP121—231) was examined using surface plasmon resonance (SPR) and compared with inhibition activities of abnormal PrP formation in scrapie-infected cells. Most examined compounds had affinities for PrP121—231: antimalarials had low affinities, whereas Congo red, phthalocyanine and thioflavin S had high affinities. The SPR binding response correlated with the inhibition activity of abnormal PrP formation. Several drugs were screened using SPR to verify the findings: propranolol was identified as a new anti-prion compound. This fact indicates that drug screenings by this assay are useful.

Key words anti-prion compound; surface plasmon resonance; scrapie-infected cell; screening; recombinant prion protein

Transmissible spongiform encephalopathies or prion diseases are fatal neurodegenerative disorders that include Creutzfeldt–Jakob disease and Gerstmann–Sträussler–Scheincker syndrome in humans, and scrapie, bovine spongiform encephalopathy and chronic wasting disease in animals. These disorders are characterized by accumulation in the brain of an abnormal isoform of prion protein (PrP), which includes a high beta-sheet content and is resistant to digestion with proteinase K.[1] Recent outbreaks of variant Creutzfeldt–Jakob disease[2] and iatrogenic Creutzfeldt–Jakob disease through use of cadaveric growth hormone or dura grafts[3] in younger people have necessitated the development of suitable therapies. Compounds such as antimalarials and amyloid binding dyes are known to possess anti-prion activity *in vitro* or *in vivo*.[4—14] Among them, Congo red and quinacrine are known to bind directly to PrP and thereby strongly inhibit proteinase K-resistant PrP (PrPres) formation.[15,16] However, it remains unclear whether or not other anti-prion compounds and amyloid binding dyes interact directly with PrP. This study analyzed interactions of some previously reported anti-prion compounds[4,7,11,17,18] and popularly used amyloid binding dyes with recombinant PrP using surface plasmon resonance (SPR). In addition, we evaluated whether SPR assay is useful as a screening tool for anti-prion compounds.

MATERIALS AND METHODS

Compounds Compounds used in the study (Fig. 1) were obtained from Sigma Aldrich Corp. (quinacrine dihydrochloride (QC, MW: 400.0), quinine hydrochloride (QN, MW: 324.4), thioflavin T (ThT, MW: 283.4, dye content 65%), thioflavin S (ThS, MW: undetermined), propranolol (MW: 295.8), promethazine hydrochloride (MW: 284.4), carbamazepine (MW: 236.3) and theophylline (MW: 180.2)), Aldrich (chloroquine diphosphate (CQ, MW: 319.9), and Congo red (CR, MW: 696.7, dye content 97%)), ICN (phthalocyanine tetrasulfonate (PcTS, MW: 922.7)), Wako Pure Chemical Industries Ltd. (Tokyo, Japan) (tetracycline hydrochloride (TC, MW: 444.4), diazepam (MW: 284.7), folic acid (MW: 441.4) and phenytoin (MW: 252.3)) or Nacalai Tesque (Tokyo, Japan) (testosterone (MW: 288.4)). All compounds were prepared as 20 mM stock solutions in water or dimethyl sulfoxide.

SPR Analysis The SPR analysis was performed using an

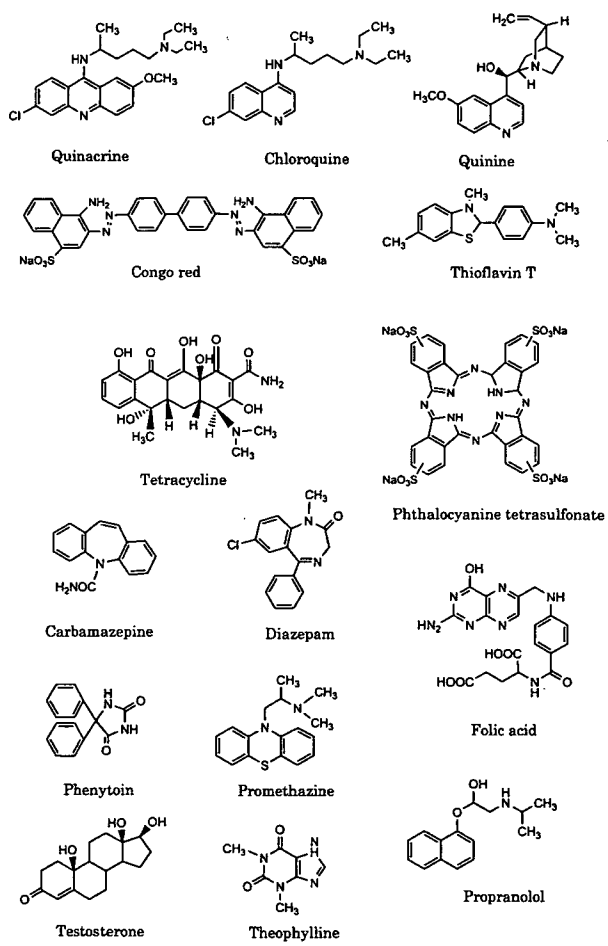

Fig. 1. Structures of Compounds or Drugs Used in the Study

* To whom correspondence should be addressed. e-mail: doh-ura@mail.tains.tohoku.ac.jp

optical biosensor (Biacore AB, Uppsala, Sweden) equipped with a CM5 sensor chip. Recombinant mouse PrP was prepared as described previously[19,20] and immobilized on a biosensor chip at a density of *ca.* 3000 resonance units (RU) using amine coupling.[21] Test compounds were diluted to 100 μM with running buffer (70 mM NaCl, 53 mM Na_2HPO_4, 12.5 mM KH_2PO_4, pH 7.4) and contained 0.5% DMSO. After they were confirmed to be in solution without precipitation or aggregation, they were injected over the PrP flow cell and the reference for either 60 s at a flow rate of 20 μl/min (low-affinity compounds) or 90 s at a flow rate of 30 μl/min (high-affinity compounds). The dissociation phase was monitored for 60 s (low-affinity compounds) or 270 s (high-affinity compounds). The flow cell was washed with 10 mM NaOH or 0.01% Triton X-100 for 30 s between each sample injection. Buffer blanks for double referencing were injected before sample analyses.[22]

The full-length recombinant of mouse PrP (residues 23—231) was used initially in the experiment, but it was easily degraded during SPR analysis in the amino-terminal portions attributable to an unidentified mechanism. For that reason, the carboxy-terminal polypeptide (residues 121—231; PrP121—231), which represents the only autonomous folding unit of PrP with a defined three-dimensional structure,[19,23,24] was used in this study.

Every PrP-immobilized biosensor chip used in the study was confirmed to respond almost the same and was standardized by the measurement of QC before its use for sample analyses.

Data Analysis The binding response, which is an index for estimating the interaction of a compound with molecules sited on a biosensor chip, is obtained from the equilibrium response (R_{eq}) value or the maximum response value in the sensorgram divided by the molecular weight.[25] In this study, the binding response of a compound was standardized by calibrating with QC, whose binding response was designated as 100 RU/Da. For low-affinity compounds, the dissociation constant (K_D) based on the R_{eq} state was calculated from data at doses ranging from 10 μM to 1 mM by either steady-state analysis using BIAevaluation software (ver. 3.0; Biacore AB) or Scatchard plot analysis. On the other hand, the K_D for high-affinity compound CR or PcTS was deduced after the data were fit to a binding model assuming a bivalent analyte in BIAevaluation software. The fitting was performed in such a way that the χ^2 value representing the statistical closeness of curve-fitting became the lowest. It was recommended ideally to be below 10.

Statistical linear correlation was evaluated using Pearson's correlation coefficient; Fisher's r to z method was used to calculate the p values. Simple linear regression analysis was also performed.

Anti-prion Activity Assay Anti-prion activity of a compound was assayed by measuring its 50% inhibition doses (IC_{50}) for PrPres formation in scrapie-infected neuroblastoma (ScNB) cells as described in previous reports.[7,11,12] Briefly, compounds were added at designated concentrations to the medium when cells were passed at 10% confluency. Cells were allowed to grow to confluence and lysed with lysis buffer (0.5% sodium deoxycholate, 0.5% Nonidet P-40, PBS). Lysates were digested with 10 μg/ml proteinase K for 30 min and centrifuged at 100000×g for 30 min at 4 °C. The pellets were resuspended in sample loading buffer and boiled. Samples were separated using electrophoresis on a 15% Tris-glycine-SDS-polyacrylamide gel and electroblotted. PrPres was detected using an antibody SAF83 (1 : 5000; SPI-Bio, France), followed by an alkaline phosphatase-conjugated secondary antibody. Immunoreactive signals were visualized using CDP-Star detection reagent (Amersham Biosciences Corp., U.S.A.) and were analyzed densitometrically. Three independent assays were performed in each experiment.

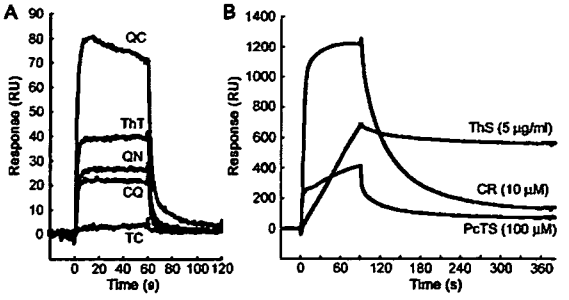

Fig. 2. Interactions of Anti-prion Compounds with PrP121—231

(A) Sensorgrams of the low-affinity compounds quinacrine (QC), chloroquine (CQ), quinine (QN), thioflavin T (ThT) and tetracycline (TC), all at 100 μM. (B) Sensorgrams of the high-affinity compounds Congo red (CR, 10 μM), phthalocyanine tetrasulfonate (PcTS, 100 μM) and thioflavin S (ThS, 5 μg/ml).

RESULTS

Interaction of Anti-prion Compounds with PrP The SPR sensorgrams of ThT and antimalarials such as QC, QN and CQ (each at 100 μM) demonstrated weak signal responses of less than 100 RU (Fig. 2A). The responses of these compounds reached equilibrium (R_{eq}) within a few seconds and returned to the baseline very rapidly after dissociation. These sensorgrams were typical for low-affinity interactions: TC showed almost no response. On the other hand, all sensorgrams of high-affinity compounds, such as CR, PcTS and ThS, showed much stronger responses and individual characteristic curves that differed from those of the low-affinity compounds (Fig. 2B). The CR (10 μM) showed the strongest signal, which was greater than 1200 RU: this decreased very slowly in the dissociation phase. The signal responses for PcTS (100 μM) and ThS (5 μg/ml) showed that neither reached the R_{eq} state within the association phase or returned to the baseline within the dissociation phase. In particular, ThS was only slightly dissociated and remained bound. This sensorgram resembled the sensorgram of biquinoline, an effective inhibitor of PrPres formation in ScNB cells (IC_{50}=3 nM).[11]

***K_D* Determination** The dose response curve for QC appeared to be monophasic and to reach a saturation level at higher concentrations; its dissociation constant (K_D) value was calculated as 1.1 mM or 0.9 mM using steady-state analysis or Scatchard plot analysis, respectively (Figs. 3A—C). Vogtherr *et al.*[16] reported the dissociation constant (K_D= 4.6 mM) of the complex of QC and human PrP 121—230 analyzed by nuclear magnetic resonance (NMR) spectroscopy. This value was almost comparable to the K_D value obtained in this study, indicating that the method used in this study was relevant. The other two low-affinity compounds, QN and